Quaternary Science Reviews 337 (2024) 108796

Contents lists available at ScienceDirect

Quaternary Science Reviews

journal homepage: www.elsevier.com/locate/quascirev

Understanding the Atlantic influence on climate and vegetation dynamics in western Iberia over the last 2000 years

Ricardo N. Santos [a,b,**], Teresa Rodrigues [b,c], Filipa Naughton [b,c], Enno Schefuß [d], Dulce Oliveira [c,b], João Moreno [e], Pedro M. Raposeiro [f,g], Graciela Gil-Romera [h], Alistair Morgan [a], Manel Leira [i], Sandra D. Gomes [b,j], S. Nemiah Ladd [a], Ricardo M. Trigo [e,k], Alexandre M. Ramos [l], Armand Hernández [m,*]

[a] Department of Environmental Sciences, University of Basel, Basel, Switzerland
[b] IPMA – Portuguese Institute of Sea and Atmosphere, Lisbon, Portugal
[c] Centre of Marine Sciences (CCMAR/CIMAR LA), Campus de Gambelas, Universidade do Algarve, 8005-139 Faro, Portugal
[d] MARUM – Center for Marine Environmental Sciences, University of Bremen, Bremen, Germany
[e] University of Lisbon, Faculty of Sciences , Instituto Dom Luiz (IDL), Lisbon, Portugal
[f] CIBIO – Associação Biopolis, Centro de Investigação em Biodiversidade e Recursos Genéticos, Pólo dos Açores, Ponta Delgada, Portugal
[g] Departamento de Biologia, Faculdade de Ciências e Tecnologia, Universidade dos Açores, Ponta Delgada, Portugal
[h] IPE-CSIC – Instituto Pirenaico de Ecología (Consejo Superior de Investigaciones Científicas), Zaragoza, Spain
[i] Department of Functional Biology (Area of Ecology), Universidade de Santiago de Compostela, Santiago de Compostela, Spain
[j] UNIARQ – Centro de Arqueologia da Universidade de Lisboa, Faculdade de Letras Universidade de Lisboa, Lisboa, Portugal
[k] Departamento de Meteorologia, Universidade Federal do Rio de Janeiro, Rio de Janeiro 1941-919, Brazil
[l] Institute of Meteorology and Climate Research Troposphere Research (IMKTRO), Karlsruhe Institute of Technology, Karlsruhe, Germany
[m] CICA – Centro Interdisciplinar de Química e Bioloxía, Universidade da Coruña, GRICA group, A Coruña, Spain

ARTICLE INFO

Handling Editor: Dr I Hendy

Keywords:
Paleoclimate
North Atlantic oscillation
Lake sediments
Lipid biomarkers
Stable isotopes
Southwestern Europe

ABSTRACT

Predicting the environmental impact of climate change in extremely sensitive areas, like western Iberia, requires an understanding of the long-term interactions between climate and vegetation. Here we present a novel high-temporal resolution multiproxy analysis, including plant-wax *n*-alkane isotope data, pollen analysis, macro-charcoal identification, chironomid and diatom records of sediments from a mountain lake in central Portugal. We examined the evolution of the Atlantic and Mediterranean climate influences over the last two millennia, exploring their connection with major atmospheric patterns and impacts on the climatic signal and vegetation dynamics in this understudied region. During the Roman Period (RP; ca. -200 – 500 AD), the study area was characterized by grass dominance, with high temperatures indicated by chironomid composition and micro-charcoal content. The increase in plant-wax δ^2H values during this period suggests a shift from wet to dry conditions. The Early Middle Ages (EMA; ca. 500–900 AD) were characterized by colder and a transition to wetter conditions, as indicated by the vegetation and plant-wax *n*-alkane isotope data. The Medieval Climate Anomaly (MCA; ca. 900–1300 AD) was generally warm, with a short initial lake level drop. This period exhibits the maximum expansion of the Mediterranean forest over the last 2 ka and possibly proximal moisture sources. During the Little Ice Age (LIA; 1300–1850 AD), a reduction of the Mediterranean forest and a strong depletion of plant-wax δ^2H values suggest cold and wet conditions with strong influence of remote Atlantic moisture, with the coldest and wettest phase of the last 2 ka detected between 1550 and 1900 AD. The post-LIA period, from 1900 AD onwards, shows a change to the present warmer and drier conditions, in a highly anthropized landscape. We also demonstrate that major changes in climate have influenced vegetation patterns, with these changes mainly controlled by large-scale atmospheric dynamics. This underscores the sensitivity of western Iberian ecosystems to climate shifts, enriches the current regional understanding of climate-vegetation interplay, and offers valuable insights for future climate change projections.

* Corresponding author.
** Corresponding author. Department of Environmental Sciences, University of Basel, Basel, Switzerland.
E-mail addresses: r.n.santos@unibas.ch (R.N. Santos), armand.hernandez@udc.es (A. Hernández).

https://doi.org/10.1016/j.quascirev.2024.108796
Received 14 May 2024; Accepted 21 June 2024
Available online 13 July 2024

1. Introduction

The Iberian Peninsula (IP) is a region of particular interest for studying present and past climate dynamics (Lionello, 2012). Located at the convergence of temperate and tropical climate systems, the regional climate is characterized by a complex orography and the influence of the North Atlantic Ocean and Mediterranean Sea. Winter rainfall, largely controlled by Hadley Circulation dynamics (i.e., tropical atmospheric circulation with air rising near the equator, descending in the subtropics, and returning equatorward near the surface) and the associated Azores High —the southern node of the North Atlantic Oscillation (NAO; Hurrell, 1995; Trigo et al., 2004)— plays a critical role in the regional ecological and economic well-being. Future climate projections indicate an amplification of the Hadley Circulation cell, leading to the expansion of the Azores High and the northward displacement of mid-latitude storm tracks and the associated jet stream. These changes are expected to result in a projected 10–20 % decline in winter precipitation by the end of the twenty-first century (Cresswell-Clay et al., 2022), making the IP one of the most vulnerable regions in Europe to ongoing global warming (Bindi and Olesen, 2011; Lionello, 2012). However, instrumental datasets are too short to include decadal-to-centennial trends and cycles, making difficult predictions at these timescales. Consequently, proxy-based reconstructions emerge as the most plausible solution to overcome this issue, being the common era (i.e., past 2 ka) a well-known period. Numerous studies have identified five significant climatic periods spanning the past two millennia in Europe: the Roman Period (RP; ca. -200 – 500 AD), the Early Middle Ages (EMA; ca. 500–900 AD), the Medieval Climate Anomaly (MCA; ca. 900–1300 AD), the Little Ice Age (LIA; ca. 1300–1850 AD), and the Industrial Era until today (1850 AD – Present) (e.g., Abrantes et al., 2017; Büntgen et al., 2021; Sánchez-López et al., 2016). The study of these periods offers invaluable insights into the sensitivity of Iberian ecosystems to changes in temperature, precipitation patterns, and atmospheric circulation dynamics. A number of previous studies have attributed climate variability primarily to fluctuations in the NAO and its impact (Morellón et al., 2011; Moreno et al., 2012), but more recent studies also suggest that other climate modes, such as the East Atlantic (EA) and Scandinavian (SCA) patterns also significantly influence climate variables in the IP (Abrantes et al., 2017; Mellado-Cano et al., 2019; Sánchez-López et al., 2016; Toney et al., 2020). However, our understanding of the major climate changes over the past 2 ka in the Atlantic region of the IP remains limited (Thatcher et al., 2020), particularly within the zone where the Eurosiberian and Mediterranean bioclimatic regions transition. Therefore, Serra da Estrela Mountain can provide valuable insights into the extent of Atlantic influence in the past climate, in both regional vegetation dynamics and continental climate.

To address this gap, we reconstruct major vegetation and climate changes over the last ca. 2 ka at decadal-to-centennial timescales in the western IP. This reconstruction employed a multiproxy approach, including the relative abundance and compound-specific stable isotope composition of plant-wax *n*-alkanes ($\delta^{13}C_{n\text{-alk}}$ and $\delta^{2}H_{n\text{-alk}}$ values), along with pollen, macrocharcoal, chironomid and diatom analyses of Lake Peixão, an alpine lake in central Portugal. Our results offer a more in-depth understanding of climatic shifts in the western IP, providing new insights into the adaptive responses of alpine ecosystems to climatic variability in a region influenced by Mediterranean and Atlantic interactions.

2. Study site

2.1. Serra da Estrela

Serra da Estrela Mountain is located in the westernmost part of the Iberian Central Range and is the highest mountain in continental Portugal (ca. 1993 m above sea level). The mountain hosts different and unique glacial features dating back to the Last Glacial Maximum (van der Knaap and van Leeuwen, 1997; Vieira, 2008; Vieira and Nieuwendam, 2020) and has recently been recognized as Estrela UNESCO Global Geopark.

Stretching in a southwest-northeast direction, Serra da Estrela acts as an important condensation barrier to the moisture-rich westerly winds, resulting in a complex interplay between Atlantic and Mediterranean climate influences (Marques et al., 2013). Due to the orographic effect and slope orientation, precipitation is higher and more frequent on the northwest slopes – influenced by the Atlantic – compared to the drier south and southeast façades, which experience a more continental and typical hot Mediterranean climate (Espinha Marques et al., 2011; Vieira, 2008). According to the vegetation-based Köppen-Geiger climate classification, the southeast side of Serra da Estela Mountain is characterized by a hot-summer Mediterranean (Csa) type, whereas the northwest side features a mild-summer Mediterranean (Csb) climate (for further details on the climate classification see Cui et al., 2021) (Fig. 1 A).

The precipitation regime in the region displays the typical bi-seasonal or interannual pattern of the western IP, where the rainy season usually lasts from October to April. This winter precipitation is mostly Atlantic-sourced (Carreira et al., 2009; Cortesi et al., 2013; Serrano et al., 1999) and highly influenced by the NAO (Ulbrich et al., 1999; Trigo et al., 2004). Historical climate data for the region (1971–2000) [see http://portaldoclima.pt/en (Accessed March 29, 2022)] reveals distinct seasonal variations. The warmest and driest months are July and August, with average temperatures around 20 °C and just 17 mm of rainfall. Conversely, December and January are the coldest and wettest months, with average temperatures of approximately 5 °C and significantly higher precipitation (150 mm) (Carreira et al., 2009, 2011). In recent decades, precipitation in Serra da Estrela mostly falls in the form of rain during autumn and spring, with snow often restricted to high altitudes during the colder winter months, when mean air temperatures typically hover around or below 0 °C (Mora, 2010). Mean annual air temperatures in the area usually remain below 7 °C, with even lower temperatures in the vicinity of the summit (Espinha Marques et al., 2011).

The combination of its climatic and geographic characteristics makes Serra da Estrela an exceptional and highly diverse region in both fauna and flora. It represents the largest natural conservation area in Portugal (Serra da Estrela Natural Park) and is recognized as an important European biodiversity hotspot (Jansen, 2011).

2.2. Lake settings

Lake Peixão (40°20′35″ N, 7°36′19″ W) is a small (0.015 km^2), subcircular alpine lake (176 m long and up to 138 m wide; 1677 m a.s.l.) located near the highest plateau of Serra da Estrela Mountain (Fig. 1 A). The origin of Lake Peixão results from the retreat of glaciers from the Serra da Estrela plateaus that occurred ca. 14.7 ± 0.32 cal ka BP (Hernández et al., 2023; Moreno et al., 2023).

Today, the lake is characterized by monomictic, oligotrophic, and slightly acidic waters (pH ~ 5.8) with a maximum depth of 5 m (Boavida and Gliwicz, 1996; Hernández et al., 2023). The catchment of the lake is constrained by steep granitic rocks, covering an area of 0.30 km^2. A drainage network composed of a few small ephemeral streams drains into the lake, and the lake outlet points to the south, allowing water to drain to the Candieira valley (Fig. 1 B) (Santos et al., 2022).

The lake surroundings are characterized by scarce and poorly developed soils, featuring an oro-Mediterranean vegetation cover composed of heathlands and grasslands. This vegetation includes shrub forms dominated by species of *Erica*, *Juniperus*, *Genista*, *Cytisus*, and *Calluna vulgaris* along with grasses like *Agrostis delicatula* and *Nardus stricta* (Connor et al., 2021; Sánchez-Mata et al., 2017; Santos et al., 2022). Other herb species such as *Potentilla erecta*, *Pedicularis sylvatica* s.l., *Festuca rubra* s.l., *Carex echinata* and *Viola palustris* subsp. *palustris* are also present in the area (Molina, 2017). The lake margins exhibit a ring of a narrow littoral zone (2–3 m) and a shallow platform to the

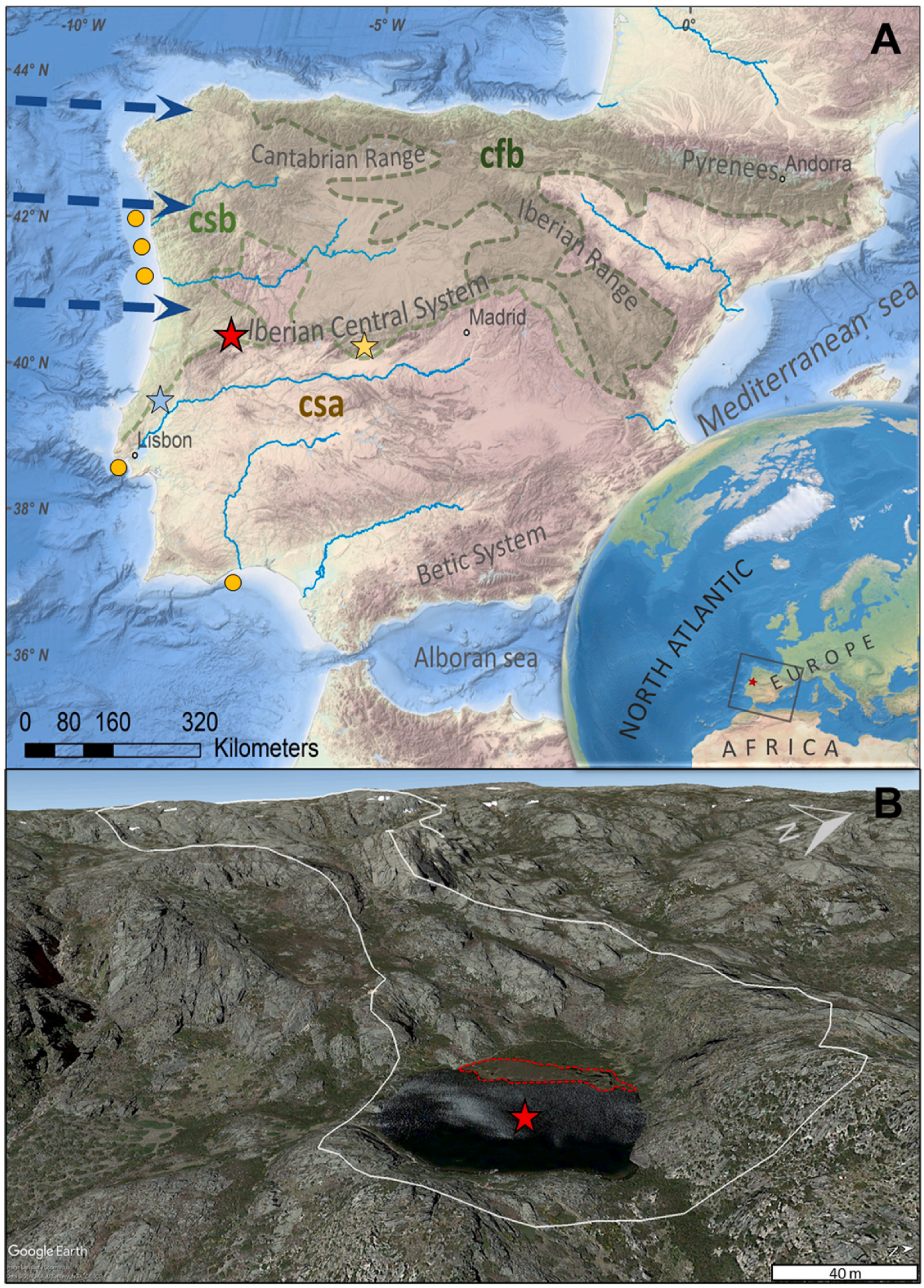

Fig. 1. Study area. A: The red star marks the location of Lake Peixão in Serra da Estrela, Portugal (adapted from Santos et al., 2022); shaded areas indicate the Köppen climate classification (csa, csb, cfb). Yellow circles mark the location of marine records used for reconstructing the Sea Surface Anomaly (Abrantes et al., 2017). The yellow star represents the location of the Cimera lacustrine record used to reconstruct the North Atlantic Oscillation index from the central Iberian Peninsula (NAO_{IP}) (Hernández et al., 2020). B: Lake Peixão (modern setting 2019). The solid white line represents the limits of the watershed; and the dashed light red line outlines the shallow floodable area in a delta-like structure; the red star represents the location of the sediment coring site of PEX19-01. Sources: The bathymetric metadata in Fig. 1A is courtesy of the EMODnet Bathymetry portal. The digital elevation model and satellite imagery from Google Earth Pro.

northwest (Fig. 1 B), with aquatic vegetation like *Antinoria-Ranunculus*, *Junco-Sphagnetum*, *Carex nigra* (L.), and *Juncus effusus* (L.) (Boavida and Gliwicz, 1996).

The contemporary fire regime is predominantly influenced by human activities, although sporadic instances of lightning-induced natural fires are occasionally observed in Portuguese mountain ranges (Tedim et al., 2013; Benali et al., 2023). Over the past decade, wildfires in the Iberian Peninsula have evolved into increasingly complex phenomena to manage. In many instances, they manifest as 6th generation fires, characterized by uncontrollable behavior that surpasses human suppression efforts and generates distinct atmospheric climate patterns (Benali et al., 2023; Campos et al., 2023). The major drivers for this change in fire regime are fuel accumulation under an increasingly warming dry season, especially in areas where human activities are frequent and therefore may trigger very large fires.

2.3. Local and regional climate drivers

The rainy season in the western IP is primarily influenced by the NAO during the winter season. The NAO is a large-scale atmospheric pattern characterized by an atmospheric pressure gradient between the Icelandic Low and the Azores High, impacting the strength and direction of moisture-rich westerly winds and storm tracks in Western Europe (e.g., Mellado-Cano et al., 2019; Trigo et al., 2004). The NAO index is

derived from the difference in normalized sea level pressure between these two regions. For negative phases (NAO^-), the atmospheric pressure gradients are less pronounced than for positive phases (NAO^+). During a NAO^- phase, storminess from the western Atlantic crosses the IP and western Mediterranean region, whereas during a NAO^+ phase, the storminess is deflected further north, affecting central and northern Europe (Hurrell, 1995; Trigo et al., 2002; Wanner et al., 2001).

However, the NAO is not the only large-scale pattern influencing climate in western and central Iberia. Other modes, such as the EA or the SCA patterns also play an important role in the climate of the IP (Hernández et al., 2015; Trigo et al., 2008). The NAO modulation by the EA can cause relevant regional weather anomalies in precipitation and in the speed and direction of the wind (e.g., Comas-Bru and Hernández, 2018; Mellado-Cano et al., 2019). Hernández et al. (2015) also highlighted that positive EA phases enhance winter precipitation and temperature, and positive SCA phases intensifying precipitation and negative SCA phases strengthening temperature.

3. Material and methods

3.1. Sediment record and chronology

We used the uppermost 149 cm of sediments from core PEX19-01, recovered from the maximum water depth area of the lake (ca. 5 m) in 2019, employing a UWITEC® Piston Corer with 60 mm wide PVC tubes. The whole sediment core is 8.5 m long and consists of homogenous dark-brown sediment with varying amounts of silt and dispersed sand grains.

The selected sedimentary section was sub-sampled for multiple analyses, including plant-wax *n*-alkanes, pollen, macrocharcoal, chironomids, and diatoms, using an adapted syringe of one cubic centimeter. Each sub-sample had a thickness of 1 cm and was labelled based on its top depth.

The age-depth model is based on a Bayesian-based model approach (Bacon v. 2.5.7; Blaauw et al., 2018), incorporating four Accelerator Mass Spectrometry ^{14}C measurements of pollen concentrate and the ^{137}Cs and ^{210}Pb profiles extracted from the upper 10 cm of the sediments (Hernández et al., 2023 and Supplementary Material Table 1). According to this age-depth model, the studied section covers the last 2.2 ka and based on mean sedimentation rate, it can be divided into four sections. From 149 to 122 cm depth, the mean sedimentation rate is 1.4 mm/year; from 121 to 78 cm depth there is a decrease to 0.89 mm/year; from 77 to 12 cm the record shows the lowest sedimentation rate (0.48 mm/year); and the uppermost part (11 cm) displays a return to higher rates, with a mean value of 0.87 mm/year.

3.2. Plant-wax n-alkanes extraction and analyses

Sedimentary plant waxes were used to infer past vegetation and climate changes in the study area for the last 2 ka. We sub-sampled a cubic centimeter sample every 2 cm, resulting in 60 sediment samples, each weighing between 0.4 and 0.6 g (dry weight). These samples were then homogenized, and 10 μl of an internal standard solution (comprising hexatriacontane, tetracontane, and nonadecanol-1-ol) was added. Samples were subjected to ultrasonic bath extraction (15 min) three times using 8 ml of dichloromethane (≥99.8%) at room temperature (21 °C) at the BioGeoChemistry Lab, IPMA in Lisbon, Portugal (see Santos, 2021). The resulting total lipid extract (TLE) was hydrolyzed with potassium hydroxide in methanol (KOH/MeOH 6 %, at room temperature overnight). The resulting neutral fraction was extracted using *n*-hexane (≥98.0%) and subsequently cleaned with ultrapure water. The apolar fraction was obtained by eluting 1 ml of the TLE over 5 cm of activated (120 °C) silica gel (0.040–0.063 mesh) in a 2 ml Pasteur pipette and purified with ca. 1.2 g of $AgNO_3$-silica gel using *n*-hexane as eluent. The *n*-alkane concentrations were analyzed with a Varian gas chromatograph Model 3800 (GC-FID) equipped with a septum programmable injector and a flame ionization detector. The concentrations of each compound were determined using hexatriacontane as internal standard (Villanueva et al., 1997).

We calculated commonly applied *n*-alkane indices to characterize the *n*-alkane distributions, including the average chain length (ACL, Poynter et al., 1989), the carbon preference index (CPI, Bray and Evans, 1961; Marzi et al., 1993), and the proportion of aquatic plants (P_{aq}, Ficken et al., 2000). These indices are used to infer general vegetation sources, degradation status, and aquatic inputs, respectively (see Supplementary Fig. 1).

Compound-specific isotope analyses of plant-wax *n*-alkanes ($\delta^{13}C_{n\text{-alk}}$ and $\delta^{2}H_{n\text{-alk}}$) were conducted using gas chromatography-isotope ratio mass spectrometry (GC-IRMS) at MARUM - Center for Marine Environmental Science, University of Bremen (Germany). The $\delta^{13}C_{n\text{-alk}}$ analysis were measured with a Thermo Trace GC Ultra coupled to a Finnigan MAT 252 mass spectrometer. The *n*-alkane extracts were injected in splitless mode before being oxidized to CO_2 by a combustion reactor at 1000 °C. The instrument was equipped with an HP-5ms capillary column (30 m × 0.25 mm × 0.25 μm film coating); helium was the carrier gas (purity 99.999%) at a constant flow of 1.5 ml/min. The produced CO_2 was then injected into the mass spectrometer for analysis. The injector temperature was maintained at a constant 250 °C, while the GC oven temperature program involved an initial hold at 120 °C for 3 min, followed by a ramp to 320 °C at a rate of 5 °C/min and a final hold for 15 min. Calibration of $\delta^{13}C$ values for individual compounds was achieved by injecting pulses of CO_2 from an external reference gas at the beginning and end of each analysis. The reported $\delta^{13}C$ values are expressed in per mil (‰) relative to the Vienna Pee Dee Belemnite (VPDB) standard and represent the average of duplicate runs whenever the amount of *n*-alkane allowed for multiple analyses. A standard deviation of less than 0.5 ‰ was maintained for these duplicate measurements.

For $\delta^{2}H_{n\text{-alk}}$, a Thermo Trace GC was employed, coupled to a Thermo Fisher MAT 253 IRMS via a pyrolysis reactor operating at 1420 °C. This setup utilized an HP-5ms column with 30 m × 0.25 mm x 0.10 μm film coating. The GC oven program employed for $\delta^{2}H$ analysis followed the conditions used for $\delta^{13}C$ analysis. To ensure measurement accuracy, standards of known isotope composition were injected after every six samples, and the H3+ factor was determined daily using H_2 reference gas (99.999% H_2 as carrier gas). Calibration of $\delta^{2}H$ values was achieved against an external H_2 reference gas, with the results reported in per mil (‰) relative to the Vienna Standard Mean Ocean Water (VSMOW) standard. Duplicate runs were performed whenever *n*-alkane quantities permitted, and the reported values represent the mean with a standard deviation of less than 3‰.

3.3. Pollen analyses

To obtain a comprehensive understanding of local-to-regional past vegetation changes and support our plant-wax signal, we analyzed pollen samples at lower resolution for the last 2.2 ka, resulting in a total of 10 pollen samples. Sample preparation, conducted at Bordeaux University (France), followed the standard protocol for marine samples detailed by Oliveira et al. (2017). The pollen extraction involved coarse sieving (150 μm mesh), consecutive treatments with cold HCl and cold HF of increasing strength, micro sieving (10 μm mesh), and slide preparation in a glycerol mobile medium. Known quantities of *Lycopodium* spores in tablet form were added to permit the estimation of pollen concentrations. Pollen analysis was carried out under a Nikon light microscope at ×500 and ×1000 (oil immersion) magnification, and identification followed European pollen atlases (Moore et al., 1991; Reille, 1992). Each pollen sample comprised 29 to 39 pollen morphotypes and reached a minimum of 350 pollen grains, excluding *Cedrus*, aquatics, and spores, to ensure a reliable representation of the vegetation community. Pollen percentages were calculated against the main sum of terrestrial grains, while aquatic pollen and spores' percentages were estimated using the total sum (pollen + spores + indeterminable + unknowns).

3.4. Macrocharcoal

Sedimentary macrocharcoal particles (charcoal particles >150 μm) were used as fire burnt biomass proxy (Clark and Royall, 1996; Marlon et al., 2012). The macrocharcoal has been proven to reflect local fire activity, i.e., at the basin scale (Higuera et al., 2010), and therefore might be related to biomass burning close to the lake. Over the last few years, innovative modelling approaches have defied the 150 μm assumption local representation (Adolf et al., 2018), however the same study conclude that it can still be used as a biomass burning proxy, especially in fuel-limited environments as mountains. The charcoal extraction of 37 samples in this study involved a chemical implied treatment of 1 cm^3 of sample. We deflocculated charcoal samples in oxygen peroxide (30 % H_2O_2) for 24h, sieved at 150 μm mesh and retrieved particles were counted on a binocular microscope (× 40). Charcoal particle identification was accomplished according to existing literature, counting opaque, angular particles (Clark and Royall, 1996; Finsinger and Tinner, 2005; Tinner and Hu, 2003; Turner et al., 2004). Counted particles were transformed to influx (particles cm^{-2} yr^{-1}) using the existing chronology (Hernández et al., 2023) and referred to as charcoal accumulation rate or CHAR.

3.5. Chironomids

For the chironomid analyses, we used 39 samples initially treated with 10 % KOH, heated to 70 °C for 5 min, sieved, and separated into two size fractions (90 and 212 μm). Head capsules were then sorted and viewed under a stereomicroscope (40× magnification – Zeiss Stemi) and mounted with Entellan® mounting medium for identification at 100x – 400× magnification (LEICA DM2500). Identification was mainly based on mentum characteristics of species morphotypes, at the lowest taxonomic resolution, using the taxonomic nomenclature of Brooks et al. (2007). The relative abundance of each taxon was presented as a percentage of the total abundance in each sample. The structure of chironomid assemblage and similarities between samples were analyzed using Principal Coordinates Ordination (PCO) with Bray-Curtis similarity. Only the PCO component related to summer temperature (PCO2) is shown here (see Moreno et al., 2023).

3.6. Diatoms frustules

We used 38 samples to determine the ratio of planktonic vs benthic diatoms to infer possible changes in lake water level, water stratification patterns, and/or eutrophic conditions. These analyses were performed at the Faculty of Sciences of the University of A Coruña, where ca. 0.3 g of dry sediment were cleaned with 30 % hydrogen peroxide (H_2O_2) and rinsed with distilled water. At least 300 diatom frustules were counted under 100× magnification to determine the relative percentage of planktonic vs. benthic diatoms.

3.7. Data analyses

We employed a Bayesian framework for a multi-source mixing model, following the methodology by Yang and Bowen (2022). This framework incorporates the BUGS language (Bayesian inference Using Gibbs Sampling) (Lunn et al., 2012), in conjunction with "rjags" package for R software and the standalone JAGS (Just Another Gibbs Sampler) encoder (Plummer, 2012). This approach uses priors (prior knowledge) that include user-defined source groups and their associated parametric relative distributions and $\delta^{13}C$ of dominant *n*-alkanes chains. The mixing process involves newly defined mixing fractions, such as fractional leaf mass contribution (FLMC) that allowed us to estimate past local dynamics of two domain vegetation groups or endmembers (grasses vs. shrubs). This reconstruction was based (prior knowledge) on the most abundant plant waxes of modern grasses and shrubs in Lake Peixão catchment (Santos et al., 2022). For that, our vegetation endmember sources relied on the abundance of the dominant *n*-C_{27}, *n*-C_{29}, and *n*-C_{31} *n*-alkanes and their carbon respective isotope values in Lake Peixão sediments.

We used Generalized Additive Models (GAMs) splines of *n*-alkane isotope records to assess long-term trends (centennial timescale) and to identify important changes over time (Simpson, 2018). For this, we used restricted maximum likelihood estimations (RMLE) and computed the first derivatives using the method of finite differences. Fitted values of the first derivative trend were obtained from each model for a grid of 200 equally spaced time points over time (last 2 ka), and we identified the periods along the fitted trend where the slope, the rate of change in the trend, was statistically significantly different from 0 (see Curtis and Simpson, 2014 for methods details). This analysis was computed using the mgcv (version 1.8–41; Wood, 2017) and gratia packages (version 0.8.1.11; Simpson, 2024) from the R software.

4. Results and interpretation

4.1. Plant-wax n-alkanes

Lipid analyses of the sediments, with a mean resolution of 30 ± 10 years between successive samples, revealed a pronounced odd-over-even carbon predominance in long-chain *n*-alkanes, specifically within the range of *n*-C_{27} to *n*-C_{35}. The abundance of these odd long-chain *n*-alkanes ranged from 60 to 150 μg/g of dry sediment) (Supplementary Fig. 1 a). These results point to a terrestrial vegetation origin, with aquatic vegetation playing a minor role.

The enclosed morphology of Lake Peixão, its oligotrophic nature, and the sparse vegetation around it make it clear that plant waxes are derived from the local vegetation cover (Santos et al., 2022). The $ACL_{27\text{-}33}$ and $CPI_{27\text{-}33}$ values remain relatively stable and elevated, ranging from 30 to 30.5 and 7.5 to 14.5, respectively (Supplementary Fig. 2 b and c). $CPI_{27\text{-}33}$ values exhibit a marked decline from the maximum to minimum values, between ca. 1740 ± 80 AD and the present, which could indicate increased soil degradation resulting from a combination of anthropogenic impact (e.g., cattle farming and land use), increased wetness and higher temperatures in the post-LIA (Pancost and Boot, 2004). Increased bacterial activity and pollution from these activities can lead to a decrease in CPI values in the uppermost sediments (Ortiz et al., 2013; Xie et al., 2004). While this observation might suggest human influence such as grazing and other land use changes, due to the current data and the nature of CPI we have considered that CPI is not robust enough to draw conclusions about anthropogenic impacts on the catchment area. The P_{aq} record displays generally low values ranging from ca. 0.1 to 0.2 (Supplementary Fig. 1 d), suggesting low contributions of waxes from aquatic plants.

The $\delta^{13}C$ values of *n*-C_{29} ($\delta^{13}C_{n\text{-}C29}$) in lake Lake Peixão sediments (Fig. 2 a; Supplementary Fig. 1 e) reinforce terrestrial vegetation as a main source of *n*-alkane plant waxes. This long-chain *n*-alkane, typically present in modern plant waxes, is abundantly produced by both shrubs and grasses in the study area (Santos et al., 2022). Besides, *n*-C29 provides a more holistic overview of the n-alkane composition of the terrestrial vegetation cover in the Lake Peixão sediments compared to *n*-C31, which may be biased towards specific species like Erica. In this context, higher $\delta^{13}C_{n\text{-}C29}$ values in Lake Peixão sediments are generally associated with shrub forms in Lake Peixão catchment, while lower $\delta^{13}C_{n\text{-}C29}$ values are associated with the grass-dominant source in Serra da Estrela (Santos et al., 2022). Nonetheless, from a vegetation source perspective we acknowledge that low $\delta^{13}C_{n\text{-}C29}$ record during a wet phase could be attributed to two potential, non-mutually exclusive, mechanisms. First, a shift towards shrub (heathland) communities, which tend to exhibit higher $\delta^{13}C$ values, while grasses show lower $\delta^{13}C$ values. Second, it could be linked to a decrease in water use efficiency of plants. Increased stomatal opening associated with wetter conditions can lead to higher ^{13}C fractionation, resulting in a decrease in the $\delta^{13}C$ values of plant-wax *n*-alkanes (Farquhar et al., 1989; Hou et al., 2007).

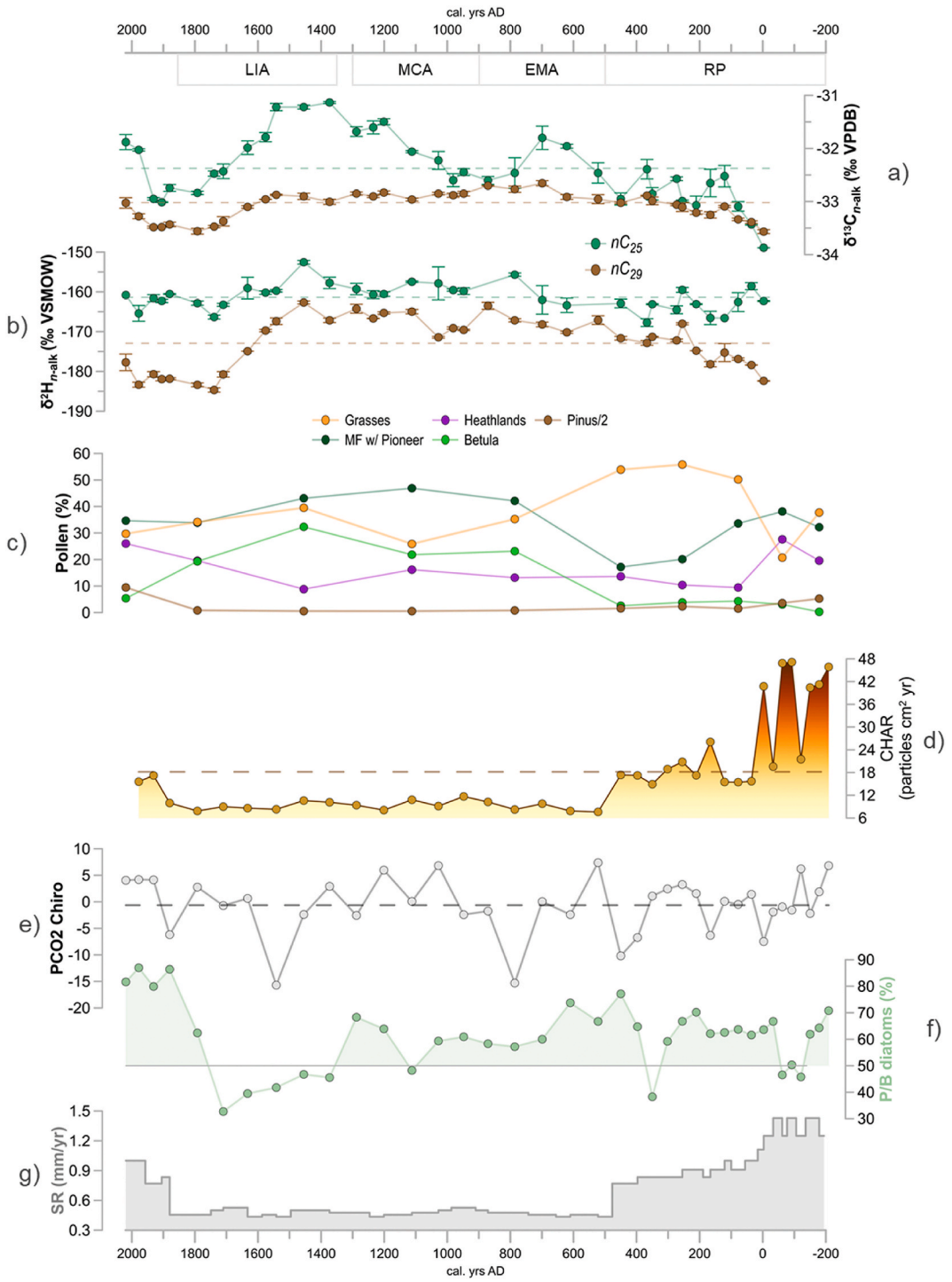

Fig. 2. – Multi-proxy data from the upper 149 cm of Pex19-01 sediment record covering the last 2.2 ka. a) $\delta^{13}C$ of *n*-C_{25} and *n*-C_{27}; b) $\delta^{2}H$ of *n*-C_{25} and *n*-C_{27} covering the last 2 ka; c) Pollen relative percentages, MF –Mediterranean forest including pioneer trees, principally Betula (birch), Pinus (50% of the total pollen counts); d) microcharcoal; e) Second component of Principle Coordinates Ordination (PCO2) of chironomid assemblage, f) Ratio between planktonic and benthic (P/B) diatoms frustules, g) Sedimentation rate (SR) based on PEX19-01 depth-age model by Hernández et al. (2023). Dashed lines represent mean values. RP – Roman Period; EMA – Early Middle Ages; MCA – Medieval Climate Anomaly; LIA – Little Ice Age.

Importantly, grasses also yield lower $\delta^{2}H_{n\text{-}C29}$ values than shrubs at this site (Fig. 2 b), adding another layer of differentiation between these vegetation types in their terrestrial vegetation source to the lake sediments (Santos et al., 2022). While FLMC analysis (Fig. 3 c) is not entirely independent from $\delta^{13}C_{n\text{-alk}}$ data, it combines the isotope signatures and *n*-alkane abundances of dominant plant-wax chains (Fig. 2 a) providing a semi-quantitative estimate of high grass-to-shrub ratio during periods predominantly characterized by low $\delta^{13}C_{n\text{-}C29}$ (Fig. 2 a).

The $\delta^{13}C_{n\text{-alk}}$ records show a notable dissimilarity between mid- and long-chain *n*-alkanes (Supplementary Fig. 1 e). The $\delta^{13}C$ values of *n*-C_{25} ($\delta^{13}C_{n\text{-}C25}$) range between −33.9 ‰ and −31.1 ‰, with an average value of −32.4 ± 0.6 ‰, while $\delta^{13}C_{n\text{-}C29}$ values are lower and more stable,

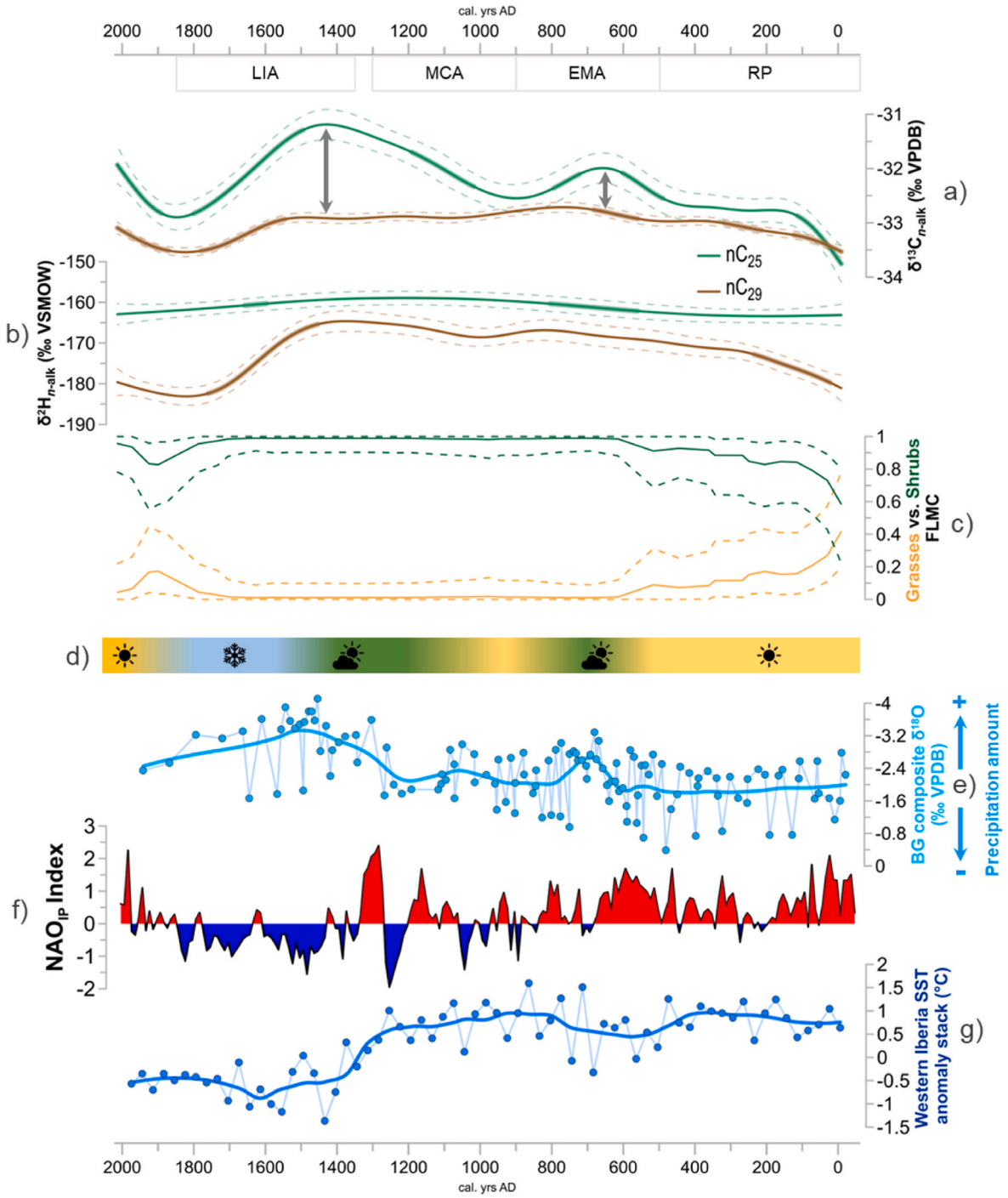

Fig. 3. Data comparison. Multidecadal trends in the upper 121 cm Pex19-01 sediment record and regional studies covering the last 2 ka; a) and b) GAM splines of $\delta^{13}C$ and $\delta^{2}H$ of n-alkane records, where the dashed lines correspond to pointwise 95% confidence intervals on the fitted smoothers, and thick sections indicate significant changes in the time series; arrows display the two main offsets between *n*-C_{25} and *n*-C_{27}; c) Estimates of fractional leaf mass contribution (FLMC) (grasses vs. shrubs) based on leaf *n*-alkanes data (relative abundances and $\delta^{13}C$ values) of dominant vegetation cover in modern settings (Santos et al., 2022); solid lines represent the maximum a posteriori estimation and dashed lines represent the 89% highest density interval of the posterior distributions; d) Conceptual model of past climate viability in Lake Peixão based on multiproxy analysis (this study); e) Composite $\delta^{18}O$ record of Buraca Gloriosa (BG) speleothem (from Thatcher et al., 2020), thick curve represents a loess smoothing curve with a span degree of 0.2; f) North Atlantic Oscillation index reconstruction from the central Iberian Peninsula (NAO_{IP}) (Hernández et al., 2020); g) Western Iberia Sea Surface Temperature (STT) stack (Abrantes et al., 2017), thick curve represents a loess smoothing curve with a span degree of 0.2. RP – Roman Period; EMA – Early Middle Ages; MCA – Medieval Climate Anomaly; LIA – Little Ice Age.

ranging from −33.6 ‰ to −32.7 ‰ (mean = −33.1 ± 0.3 ‰) (Figs. 2 a and Fig. 3 b). There are two main intervals with evident offsets of 1 ‰ and 2 ‰ between $\delta^{13}C_{n\text{-}C25}$ and $\delta^{13}C_{n\text{-}C29}$ values, occurring between 550 ± 90 AD to 830 ± 140 AD and 1030 ± 160 AD to 1700 ± 100 AD, respectively (Fig. 3 a). High $\delta^{13}C$ values in mid-chain *n*-alkanes are commonly linked to aquatic plants (e.g., Aichner et al., 2018, 2010). In the catchment of Lake Peixão, *Juncus* type and terrestrial plants, including *Cytisus* and *Agrostis*, can also produce significant amounts of *n*-C_{25} (Santos et al., 2022). We thus interpret a larger offset between *n*-C_{25} and *n*-C_{29} $\delta^{13}C$ values as indicative of an increased contribution of

n-C_{25} from aquatic plants during these periods, with *n*-C_{29} in Lake Peixão sediments mainly sourced from terrestrial plants, and *n*-C_{25} representing a mixed signal from terrestrial and aquatic plants.

The δ^2H records show some intervals with differences between *n*-alkane homologues (Fig. 2 a, b, and Supplementary Fig. 1 f). The δ^2H values of *n*-C_{25} ($\delta^2H_{n\text{-}C25}$) remain mostly constant, ranging from −168 ‰ to −153 ‰ (mean = −161 ± 3 ‰), whereas δ^2H values of *n*C_{29} ($\delta^2H_{n\text{-}C29}$) values are lower, ranging from −185 to −163 ‰ (mean = −173 ± 7 ‰) (Fig. 2 b). The $\delta^2H_{n\text{-}C29}$ values increase from ca. 0 ± 50 AD to 300 ± 70 AD and then remain rather stable until the interval encompassing 1450 ± 120 AD to 1740 ± 80 AD, where they decrease. Under a consistent vegetation source, changes in $\delta^2H_{n\text{-}C29}$ values are usually associated with variations in local precipitation δ^2H values (Sachse et al., 2012), which are mainly dependent on rainfall amount/intensity, condensation temperature, and isotope signatures of moisture sources (Bowen et al., 2019; Cheddadi et al., 2021; García-Alix et al., 2021). In the study area low (high) δ^2H values can be linked to a combination of high (low) precipitation amount and remote (local) atmospheric moisture sources (see Santos et al., 2022). An additional secondary influence on $\delta^2H_{n\text{-}C29}$ values can be due to vegetation changes, with grasses in the catchment area having significantly lower values than shrubs (Santos et al., 2022), consistent with global observations (Kahmen et al., 2013; Liu and An, 2019). However, the FLMC analyses indicate relatively stable inputs of *n*-alkanes from grasses relative to shrubs throughout most of the Lake Peixão record, including the large decline in $\delta^2H_{n\text{-}C29}$ values (ca. 20 ‰) during the LIA, and we thus interpret these changes as shifts in precipitation δ^2H values.

4.2. Pollen record and macrocharcoal

The pollen record has a time resolution of 260 ± 84 years between samples, while the macrocharcoal record (biomass burning) has an average of 60 ± 20 years resolution. Pollen analyses revealed a consistent presence of oro-Mediterranean vegetation, dominated by *Poaceae* (grasses), heathlands (*Ericaceae* and *Calluna*-type) and Mediterranean forest (MF) (Fig. 2 c). The MF is mainly composed of *Betula* and *Quercus* deciduous, but also includes some thermomediterranean to supra-mediterranean taxa such as *Acer*, *Alnus*, *Corylus*, Cupressaceae, *Fraxinus excelsior* type, *Ulmus*, *Quercus* evergreen type, *Quercus suber* type, *Cistus*, *Coriaria*, *Myrtifolia*, *Olea*, *Phillyrea*, and *Pistacia*. This vegetation cover usually expands in the IP when the climate is warm/temperate and humid (e.g., Chabaud et al., 2014; Naughton et al., 2019) The heathlands are represented by both *Ericaceae* and *Calluna* and usually develop under moist conditions, albeit relatively drier than those of MF expansion (e.g., Chabaud et al., 2014; Fagúndez and Pontevedra-Pombal, 2022). In contrast, grasses typically expand under relatively dry conditions (e.g., Carrión et al., 2010, 2001; Jalut et al., 2000; Naughton et al., 2016). Although human activities have been evident in the nearby Charco da Candieira lake for the last 2 ka, as indicated by the presence of *Castanea* (chestnut) in the pollen record, they do not mask the natural vegetation signal (Connor et al., 2012).

The comparison between the Lake Peixão pollen record and macrocharcoal concentrations profile from the same core allow us to distinguish several intervals: From −180 ± 70 AD to 0 ± 50 AD the vegetation cover in Lake Peixão suggest an evenly distribution of heathlands, MF and grasses, while showing highest macrocharcoal concentrations of 38 ± 11 particles/cm^2yr. The burning pattern between ca −200 and 100 AD seems to be connected to the existence of heathlands that have evidenced in other mountain areas of the world to have long-term clear resilient responses to fire through post fire strategies as resprouting (Gil-Romera et al., 2019; Schwörer et al, nd). The burning biomass at that time would then be more linked to woody vegetation wildfires that, under a fire conducive climate, i.e., a dry, warm season, would trigger larger, more intense fires. From 0 ± 50 AD to 450 ± 50 AD, grasses expanded (ca. 55%), and the relatively low abundances of heathlands and MF, suggesting a dry climate (Fig. 2 c). This period is distinguished by progressively lower fire activity (macrocharcoal concentrations of 20 ± 6 particles/cm^2yr, Fig. 2d), probably due to a collapsing woody plant community that, therefore, would prevent large wildfires to happen, despite climate conditions may have facilitated burning to spread. The landscape change observed ca. 100 AD supports certain degree of seasonality as fire activity is still present, while the forest tends to decline. We cannot discard that local human action would have facilitated the observed fires between −200 and 450 AD, however there is no additional clear indicator of human activity on the vegetation assemblages supporting this alternative.

From 450 ± 50 AD to 1460 ± 150 AD, MF witnessed a relative expansion in the region (increasing to 40%), primarily at the expense of grassland areas. This change suggests a shift towards relatively temperate/warm and moist environmental conditions. Although MF remained prevalent from 1460 ± 150 AD to the present, there was a notable decline in *Betula*, coupled with a progressive increase in heathlands (reaching up to 30%) (Fig. 2 c). This increase in heathlands suggest that climate remained relatively moist throughout the year (Fagúndez and Pontevedra-Pombal, 2022). The CHAR record consistently showed low values, approximately 8 particles/cm^2yr. However, an increase to around 18 particles/cm^2yr was observed between 1880 ± 30 AD and the present day. This increase is likely linked to a significant expansion of *Pinus,* promoting biomass available for burning, and human-induced changes on landscape that can promote fire-prone conditions.

4.3. Chironomid-based spring-summer temperatures

The chironomid record has a temporal resolution of 60 ± 20 years and evidence of a total of 36 taxa belonging to four subfamilies, with the dominant *Chironomus plumosus* type constantly present throughout the record. However, the second-most dominant type, *Chironomus anthracinus* type was mainly constrained between 1540 ± 130 AD to 700 ± 120 AD interval. The overall chironomid assemblage suggests that the lake persisted as relatively shallow and oligo-to mesotrophic throughout the studied interval, with PCO_2 mainly explaining spring-summer temperature-related variance (Fig. 2 e) (Moreno et al., 2023). The PCO_2 curve shows two main intervals where the values are generally below or very close to the record average of the studied section, the first ranging from 620 ± 100 AD to 1000 ± 155 AD (Fig. 2 e) and the second from 1455 ± 130 AD to 1710 ± 90 AD.

4.4. Planktonic vs. benthic diatoms (P/B)

The diatom record of the studied section has a temporal resolution of 60 ± 20 years. The diatom flora is dominated by planktonic forms, with the *Aulacoseira* being the most abundant genus. In contrast, benthic diatoms show higher diversity and are primarily represented by *Eunotia*, *Pinnularia*, and *Gomphonema*. Throughout most of the record, planktonic forms dominated, with P/B values ranging from 33 to 87% (Fig. 2 f). Between −200 ± 80 AD to 400 ± 60 AD, the P/B value is ca. 60%, with short intervals of lower values around −100 AD and 300 AD. After 400 AD the P/B ratio increased to values around 65% that lasted until 700 ± 120 AD. This is followed by an interval where P/B values slightly drop and remain relatively constant around 60% until 1300 AD, followed by a short increase in P/B values. From 1290 ± 160 AD to 1630 ± 120 AD, the diatom values show a decrease in planktonic taxa, with P/B values dropping below 50%. The lowest value was recorded at 1630 ± 120 AD, however, from this time to the present, there was a pronounced increase in P/B values, reaching the highest value (ca. 85%) (Fig. 2 f).

The P/B record of lake sediments can reflect a range of environmental factors (e.g., Leira et al., 2009; Leira and Sabater, 2005; Pienitz et al., 1995; Scussolini et al., 2011). We consider the small size and shallow depth of the lake as critical factors. These characteristics make the lake more sensitive to climate changes due to reduced water volume and depth, which would otherwise buffer against temperature and

precipitation changes (Gerten and Adrian, 2001; Råman Vinnå et al., 2021). As a result, the P/B ratio in a small lake such as Lake Peixão is likely to be responsive to climatic changes, with high (low) values usually linked with high (low) lake levels. This sensitivity is evidenced by the P/B responses to observed productivity and warming trends, stratification, and high sedimentation rates. In this study, we compare the P/B ratio with other proxy records to support the interpretations of the Lake Peixão dynamics (see Fig. 2).

5. Discussion

5.1. Vegetation and climate reconstruction over the last 2 ka

5.1.1. 'Roman Period' (RP, ca. −200 to 500 AD)

The concurrent low $\delta^{13}C$ values of *n*-C_{29} and *n*-C_{25} in Lake Peixão sediments point to a considerable contribution from grasses, or low water use efficiency (see Santos et al., 2022), to the *n*-alkane pool during the RP. This aligns with the high grass-to-shrub ratio in the FLMC and pollen data (Figs. 2 c and 3 c). Despite previous studies have associated the expansion of grasses in the IP with more arid conditions (e.g. Carrión et al., 2010, 2001; Jalut et al., 2000; Naughton et al., 2016), grasses and wet conditions also matches with the nowadays ecology in that particular area (Santos et al., 2022). Nonetheless, we acknowledge that plant waxes in the lake sediments can result not solely directly from vegetation but also pass through the soil layer with soil erosion and input into the lake a secondary source (Wiesenberg et al., 2004). This can lead to a smoothing effect in the recorded climatic signal. Therefore, the above-mentioned increase in the abundance of grasses from 0 ± 50 AD and increasing trend in $\delta^{2}H_{n\text{-}C29}$ values during this period might indicate a shift towards a drier RP climate with a declining influence of the remote Atlantic moisture source. Nonetheless, the timing of this change could be slightly delayed by the influence of reworked soil organic matter due to high run-off events, evidenced by high sedimentation rates (Fig. 2 g).

The progressively declining forest would have resulted in a reducing intensity of wildfires compared to the previous period (−200 to 100 AD) implying either smaller or less intense fires during this period (Fig. 2 b, d). These burning patterns, in possibly a mosaic landscape with reducing woody plant communities and expanding grasslands, would support drying condition, at least seasonally. The prevalence of these conditions is supported by the composite $\delta^{18}O$ speleothem record of Buraca Gloriosa from central Portugal (Fig. 3 e) (Thatcher et al., 2020). Arid conditions are reconstructed from several NW marine and continental records (e.g., Bernárdez et al., 2008; Jambrina-Enríquez et al., 2014), whereas moist conditions or fluctuating wet/dry cycles, are reported in other IP studies (Bartolomé et al., 2024; Corella et al., 2013; Gázquez et al., 2020; López-Avilés et al., 2021; Sánchez-López et al., 2016).

Warm conditions during the RWP at Lake Peixão are evident from chironomid data, indicating positive spring-summer temperature anomalies (Fig. 2 e). Similar warm conditions have been reported in the alkenone-based Sea Surface Temperature (SST) Stack record of the western Iberian margin (Fig. 3 g) and various IP records (Desprat et al., 2003; Fletcher et al., 2012; Martín-Chivelet et al., 2011; Thatcher et al., 2020).

The warm and increasingly drier climate of the RP contributed to a declining woody vegetation that combined with frequent and/or intense wildfires, may have promoted open vegetation landscapes, soil erosion, and intense runoff events likely due to snow melting in a warmer climate. This can support a strong climate contrast between wet and dry seasons during this period (Fig. 2 g). Furthermore, these climatic conditions likely led to a decrease in the lake level shown by the P/B ratio.

5.1.2. Early Medieval ages (EMA, ca. 500–900 AD)

During this interval, the $\delta^{13}C_{n\text{-}C29}$ values slightly increase, reflecting the relative reduction of grasses in the vegetation cover or increase in the water use efficiency of plants in the catchment (Fig. 2 c; 3 a, c). The contraction of grasses is further supported by the decrease in the grass-to-shrub ratio and *Poaceae* percentages in the pollen diagram of Lake Peixão (Figs. 3 c and Fig. 2 c). The offset between the $\delta^{13}C_{n\text{-}C25}$ and $\delta^{13}C_{n\text{-}C29,}$ detected during the EMA interval, with its maximum at the mid-EMA (ca. 650 AD), indicates the expansion of aquatic plants in the Lake Peixão (Fig. 3 a). The observed relative expansion of MF (Fig. 2 c) and the concurrent reduction in grasslands around Lake Peixão suggest precipitation distributed throughout the year (i.e., less seasonal). The substantial change in the forest cover in the region is consistent with findings from the Charco da Candieira (van der Knaap and Van Leeuwen, 1995; Connor et al., 2012). Additionally, a simultaneous change (decrease) in the wildfire regime (Fig. 3 d).

Evidence of changes in precipitation patterns during this period is also found in the $\delta^{18}O$ of Buraca Gloriosa speleothem record, in central Portugal (Fig. 3 e) (Thatcher et al., 2020). The increase in $\delta^{2}H_{n\text{-}C29}$ values from the RP to the EMA is likely indicative of the significant shift in the hydroclimate with a change in the hydrological regime, a more proximal moisture source and possibly link to the expansion of shrub and nearshore aquatic plants (see Santos et al., 2022). This overall increased moisture availability from RP to EMA at Lake Peixão is similar to other records of the northwestern IP (e.g., Jambrina-Enríquez et al., 2014; Álvarez et al., 2005; Desprat et al., 2003).

Chironomid data indicate complex summer temperature patterns, with an initial rapid increase followed by a gradual cooling, reaching its lowest value around 800 AD (Fig. 2 e). Despite a slight decrease in temperatures post-mid EMA, forest cover did not significantly decline. The SST stack curve indicates only a modest mean decrease of 1 °C (Fig. 3 g) (Abrantes et al., 2017), insufficient to trigger a noticeable reduction in forest cover (Connor et al., 2012; Naughton et al., 2007). This pattern is consistent with other northwestern and central IP records, which also indicate a relatively homogenous pattern of colder conditions during the EMA (Álvarez et al., 2005; Desprat et al., 2003; Gil García et al., 2007; Jambrina-Enríquez et al., 2014; López-Merino et al., 2009).

5.1.3. Medieval climate anomaly (MCA, 900–1300 AD)

The onset of the MCA (900–1000 AD) is characterized by a very low offset between $\delta^{13}C_{n\text{-}C25}$ and $\delta^{13}C_{n\text{-}C29}$ (Figs. 2 and 3 a). This indicates that during the transition between EMA and MCA, aquatic plants reduced significantly, while shrubs dominated over grasses (Figs. 2 and 3 a). However, forested vegetation in the region is still dominated by MF, reflecting sufficient moisture availability. The $\delta^{2}H_{n\text{-}C29}$ record shows minimal variation during the MCA, suggesting low precipitation and stable hydroclimate seasonal patterns, proximal moisture sources and a strong resilience of terrestrial vegetation.

An increase in chironomid-based summer temperatures marks the beginning of the MCA (Fig. 2 e), corroborated by similar trends in the western Iberian margin SST-Stack (Fig. 3 f). The elevated MF (Fig. 2 c) and the warming pattern, noted in several IP records (e.g., Martín-Chivelet et al., 2011; Moreno et al., 2012; Sánchez-López et al., 2016), further support warm temperatures.

After the onset of the MCA, $\delta^{13}C_{n\text{-}C25}$ values start to increase, while $\delta^{13}C_{n\text{-}C29}$ values remain constant until the end of the MCA, resulting in an increase of the offset between these values (Figs. 2 a, and 3 a). This increase in the offset suggests a potential reemergence of aquatic plants, which can be linked with changes in lake level. However, we acknowledge that interpreting the link between aquatic inputs and lake level changes can be questionable under such low P_{aq} values (Supplementary Fig. 1 d) and low $\delta^{13}C$ offsets (ca. 1.5–2 ‰).

Chironomid-based temperature data show a continued rise, peaking at ca. 1100 AD, followed by a slight decline towards the late MCA (Fig. 2 e). In other IP records, particularly from the south, the MCA is also typically associated with dry and warm conditions (e.g., García-Alix et al., 2020; López-Avilés et al., 2021; Martín-Puertas et al., 2008; Moreno et al., 2012; Sánchez-López et al., 2016). Moreover, Buraca Gloriosa speleothem also recorded low precipitation through most of the

MCA (Fig. 3 e), whereas wet conditions were recorded in northwestern IP (Álvarez et al., 2005; Desprat et al., 2003). Documentary sources report a high flood frequency in major Iberian rivers after 1200 AD at the end of MCA (Benito et al., 2003).

5.1.4. Little Ice Age (LIA, 1300–1850 AD)

The beginning of the LIA is characterized by a pronounced offset in the $\delta^{13}C$ values between *n*-C_{25} and *n*-C_{29} values, coupled with an increase in *Betula* abundance (Figs. 2 and 3 a). Concurrently, there is a notable decline in Chironomid-based temperature data and a sustained decrease in the P/B ratio (also indicating less stratified lake waters) (Fig. 2 f). These patterns are likely indicative of a colder climate period as suggested by Lei et al. (2021) and Rühland et al. (2008, 2003). Additionally, the SST stack of western Iberia exhibits a significant decline (Fig. 3 g), further corroborating the evidence of a major cooling trend during this period.

After 1500 AD, a significant decrease in temperatures prompted a clear reduction in aquatic plants and P/B ratio (Figs. 2 and 3 a), possibly linked to prolonged freezing conditions in the lake. Given that the local terrestrial vegetation remained relatively consistent (Figs. 2 and 3 c), the largest decline in the $\delta^2H_{n\text{-}C29}$ values through the studied record occurred, showing that the LIA climate changes had more pronounced effects than the variability associated with earlier periods in the past 2ka. This depletion of $\delta^2H_{n\text{-}C29}$ values was likely primarily driven by an increase in: i) rainfall, ii) seasonality, and iii) remote Atlantic moisture sources (Fig. 3 b). The decreasing presence of MF and *Betula*, along with a 10 % rise in heathlands (Fig. 2 c), further emphasizes the prolonged cold and wet conditions experienced during the LIA in western Iberia.

This increase in rainfall is also recorded in the $\delta^{18}O$ of Buraca Gloriosa speleothem (Fig. 3 e) and is consistent with other regional studies reporting intensified river outflows (e.g., Abrantes et al., 2017). The transition from mild and wet to cold and wet conditions during the LIA agrees with numerous records across the IP, highlighting the significant regional impact of the LIA (e.g., García-Alix et al., 2020; Moreno et al., 2012; Oliva et al., 2018; Sánchez-López et al., 2016; Thatcher et al., 2023).

5.1.5. Post-LIA to modern (ca. 1850 AD – present)

In the uppermost sediments of Lake Peixão, there is a pronounced environmental shift post-LIA. The plant-wax $\delta^{13}C$ records show increasing values (Figs. 2 and 3 a), suggesting a change in lake levels or a eutrophication process due to cattle grazing in the lake catchment. This period is characterized by a substantial rise in SRs due to changes in rainfall patterns (e.g. larger differences between winter and summer) or, more likely, an impact of grazing and erosion by cattle and human induced land-use changes that also influenced the development of grasses (Figs. 2 g and 3 c).

Additionally, warmer post-LIA conditions could have promoted water column stratification, thereby favoring the increase of planktonic diatoms, consistent with the observed increase in the P/B ratio after the LIA (see Fig. 2 f). However, changes in the diatom and chironomid records during this phase may reflect not only environmental alterations but also the impact of human activities, such as changes in the trophic level of the lake (Vázquez-Loureiro et al., 2023). The dramatic increase in SR (Fig. 2 g), alongside palynological and macrocharcoal records, further suggests both warming and a rise in human activities at a regional level. This is supported by the intensification of wildfires (i.e., increase in macrocharcoal), possible as a result in more available biomass or continuous deforestation of the natural deciduous forests, and an increase in pine due to human intervention (Fig. 2 c, d). Indeed, the substantial human impact, including agropastoral practices like grazing, fire management, and afforestation with species such as pines, olive trees, and *Cerealia*, is well-documented in the region (Connor et al., 2012; van der Knaap and van Leeuwen, 1995).

The post-LIA period also records a slight rise in $\delta^2H_{n\text{-}C29}$ values, suggesting a drying trend linked with the decline in lake levels until today. This warming and drying trend aligns with the current observations and projections for the region for this period (Sousa et al., 2020).

Overall, the post-LIA conditions at Lake Peixão are characterized by the increase in temperature, aridity, and significant human-driven changes. These findings are in line with other records from the IP for this time interval, highlighting widespread environmental and anthropogenic influences (López-Avilés et al., 2022; Sánchez-López et al., 2016; Thatcher et al., 2020).

5.2. Climate regime shifts and impact of large-scale atmospheric patterns

The climate evolution of the central western IP over the past 2 ka is less well-known in comparison to other regions of the IP. Climate changes and the resulting variation in vegetation in this region are most likely triggered by the decadal-to-centennial changes in the Atlantic moisture sources influenced by changes in seasonality and the relative contributions of remote versus proximal moisture sources via large-scale atmospheric patterns.

During the RP, the prevailing NAO + conditions (Fig. 3 f) support evidence of local warm and a transition from wet to arid conditions (Fig. 3 d), likely influenced by a change from more Atlantic climate conditions to a higher influence of Mediterranean climate (Csa) conditions on regional scale. The NAO values remained mostly positive throughout the EMA (ca. 500–900 AD). These conditions gradually shifted towards a more neutral NAO (index ranging from ca. −0.5 to 0.5) and even negative values at the beginning of MCA (Fig. 3 f). We suggest a change to wetter conditions from the end of the RP and the onset of the EMA towards the EMA-MCA transition (Fig. 3 d). This hydroclimate transition may be associated with less extreme NAO phases (Fig. 3 f) and modulated by a shift from positive to negative EA phases (Mellado-Cano et al., 2019). This could also explain the contrasting climate conditions between the northern/western and southern/eastern Iberian regions during most of the EMA (Sánchez-López et al., 2016). Specifically, the northern/western regions, which were predominantly cold and wet, experienced a more pronounced Atlantic influence (Csb), whereas the southern/eastern regions experienced generally warm and dry conditions. The MCA (900–1300 AD) in the study area started with a short lake level change event, changing to wetter conditions after 1000 AD. These two MCA stages (Fig. 3 d) with a change from dry to wet conditions are also reflected on the NAO evolution, which showed positive and negative phases, respectively (Fig, 3 f). Apparently, a larger persistence of the Mediterranean climate (Csa) conditions in the Lake Peixão region would define the MCA, resulting in maximum expansion of the MF.

During the early LIA, consistently negative NAO values induced wet conditions (Fig. 3). The transition from the early LIA (ca. 1350–1450 AD) to the late LIA (1450 AD to 1900 AD) represents a change to colder conditions (Figs. 2 b, 3 b d) reflecting a strong change in the local climate. This transition is likely related to a shift from EA^+ to EA^-, even under strong negative NAO conditions (Mellado-Cano et al., 2019; Zubiate et al., 2017). These findings suggest that the cold and wet conditions during the latter part of the LIA (Fig. 3 d) can be associated with the southward position of the jet stream under a weakened polar vortex (Mellado-Cano et al., 2019). This resulted in strong Atlantic climate conditions and a contraction of some vegetation, like MF, in comparison with the MCA. This shift enhanced the impact of moisture sources with lower isotope values in the region (Taylor et al., 2018), imprinting the decrease in $\delta^2H_{n\text{-alk}}$ values observed in Lake Peixão sediments (Fig. 2).

Finally, following the LIA (from 1900 AD to the present), despite the human overprint in the proxy-based climate signal (Sánchez-López et al., 2016), a transition to warmer and drier conditions is observed (Fig. 3 d), accompanied by a global trend of wind stilling (McVicar et al., 2012; Tian et al., 2019). Correspondingly, NAO values changed from mostly negative to mostly positive (Fig. 3 f), the EA from negative to positive (Comas-Bru and Hernández, 2018; Comas-Bru and McDermott,

2014; Mellado-Cano et al., 2019) and the SCA from positive to negative (Comas-Bru and Hernández, 2018; Hernández et al., 2015). These changes likely resulted in an increase in the persistence of the hot Mediterranean climate (Csa) conditions that persist until today.

Hence, our results support the primary influence of the NAO and the secondary influence of other two main modes of climate variability in this region (i.e., EA and SCA) on the vegetation and organic geochemistry of alpine ecosystems in the IP, as observed in previous works (e.g., García-Alix et al., 2017; Jiménez-Moreno et al., 2013; López-Avilés et al., 2021). However, our findings highlight that the NAO-driven changes in Lake Peixão are mainly evident during strong NAO phases over centennial timescales. This indicates that the relationship between hydroclimate and vegetation dynamics in central western IP can be intricate and regionally constrained. Thus, we support earlier studies emphasizing the importance of large-scale atmospheric patterns and their regional teleconnections, such as the NAO, EA, and SCA, in understanding the complexity of Iberian climate (e.g., Abrantes et al., 2017; Hernández et al., 2015; Trigo et al., 2008).

6. Conclusions

Our study revealed pronounced climate and environmental changes in Lake Peixão over the past 2 ka. The multi-proxy approach reconstruction applied highlighted the potential to overcome the limitations of the individual proxies and reveal the main shifts in vegetation and hydroclimate dynamics in the region. These results suggest that during the RP (ca. -200 – 500 AD), grasses were an important component of the vegetation cover in Serra da Estrela which experienced intense fires. The climate was warm following a trend from wet (−200 – 0 AD) to dry conditions (0–500 AD) under prevailing NAO+ and more Mediterranean influenced climate. During the EMA (ca. 500–900 AD), proxy-based data suggest a progressive decrease in Mediterranean climate influence, potentially due to the influence of positive to neutral NAO phases modulated by the EA, resulting in a transition to wet conditions, a dominance of shrubs forms in the vegetation cover and a decrease in fire regime. The MCA (ca. 900–1300 AD) shows an initial lake level drop and the largest expansion of MF and variability in aquatic production in the lake, as well as an oscillating NAO behaviour, along with the persistence of warm Mediterranean climate conditions. The LIA was a general cold and wet period, under a persistent negative NAO phase. After an early mild phase (1350–1550 AD), the late LIA and the onset of the Industrial period (1550–1900 AD), was the coldest period of the last 2 ka, as the result of a shift from EA + to EA-under strong negative NAO conditions. These conditions likely triggered a decline in the MF under a more Atlantic influence. Following the LIA, from 1900 AD to the present, increasing human impact is detected with a transition to warmer and drier climate, such as increase in biomass burning and increase in grasses, resulting in changes in the aquatic inputs or lake trophic level. The NAO values shifted from mostly negative to positive modulated by the EA and SCA patterns, under the influence of the current hot Mediterranean climate.

This study provides new insights into the centennial-scale trends of vegetation and climate dynamics in the western IP. Over these timescales, the NAO exerted a primary influence on these dynamics, while the EA and SCA played secondary roles. Our findings underscore the complexity of the IP climate during the last 2 ka, particularly notable in periods beyond the 2 ka where existing reconstructions are fewer and yield more variable results. Thus, new studies to improve our understanding of the western IP climate and vegetation evolution beyond the last millennium will be highly valuable.

Funding

The coring campaign was supported by the Portuguese Foundation for Science and Technology – FCT, through the HOLMODRIVE project (PTDC/CTA-GEO/29029/2017), and laboratory work supported by the WarmWorld project (PTDC/CTA-GEO/29897/2017). RNS's grant is supported by the FCT Ultimatum project (IF/01489/2015) and WarmWorld; IPMA's Biogeochemistry Lab equipment was supported by EMSO-PT - PINFRA/22157/2016. DO, TR and FN, acknowledge funding from FCT through the CCMAR FCT Research Unit—project UIDB/04326/2020 and Hydroshifts (PTDC/CTA-CLI/4297/2021). DO is also funded through the contract (CEECIND/02208/2017). AH is funded by the Spanish Ministry of Science and Innovation through the Ramón y Cajal Scheme [RYC2020-029253-I]. AMR was supported by the Helmholtz 'Changing Earth' program.

Authors contribution

RNS: conceptualization; methodology; investigation; formal analysis; writing – initial draft; writing – reviewing and editing. TR: conceptualization; methodology; investigation; formal analysis; Supervision; writing – initial draft; writing – reviewing and editing; funding acquisition. FN: conceptualization; methodology; investigation; writing – initial draft; writing – reviewing and editing; ES: conceptualization; methodology; investigation; formal analysis; writing – reviewing and editing; funding acquisition. DO: methodology; investigation; writing – reviewing and editing; JM: methodology; investigation; writing – reviewing and editing; PR: methodology; formal analysis; investigation; writing – reviewing and editing. GGR: methodology; investigation; formal analysis; writing – reviewing and editing. AM: writing – reviewing and editing. ML: methodology; investigation; formal analysis; writing – reviewing and editing. SDG: methodology; writing – reviewing and editing. SNL: conceptualization; methodology; investigation; writing – initial draft; writing – reviewing and editing. RMT: investigation; writing – reviewing and editing. AMR: investigation; writing – reviewing and editing; Supervision; project administration AH: conceptualization; funding acquisition; Supervision; methodology; investigation; writing – initial draft; writing – reviewing and editing.

Declaration of competing interest

The authors declare that they have no known competing financial interests or personal relationships that could have appeared to influence the work reported in this paper.

Data availability

Data will be made available on request and PANGAEA.

Acknowledgements

We are thankful to Mária Padilha for the help in *n*-alkane extraction at BGQ_Lab, IPMA and Ralph Kreutz for the CSIA at MARUM. Pedro JM Costa, Alberto Sáez, Santiago Giralt and personal of the Estrela UNESCO Global Geopark for field work during coring campaign. We thank Pepe Carrión and an anonymous reviewer for their kind and helpful comments.

Appendix A. Supplementary data

Supplementary data to this article can be found online at https://doi.org/10.1016/j.quascirev.2024.108796.

References

Abrantes, F., Rodrigues, T., Rufino, M., Salgueiro, E., Oliveira, D., Gomes, S., Oliveira, P., Costa, A., Mil-Homens, M., Drago, T., Naughton, F., 2017. The climate of the common era off the iberian peninsula. Clim. Past 13, 1901–1918. https://doi.org/10.5194/cp-13-1901-2017.

Adolf, C., Wunderle, S., Colombaroli, D., Weber, H., Gobet, E., Heiri, O., van Leeuwen, J. F.N., Bigler, C., Connor, S.E., Gałka, M., La Mantia, T., Makhortykh, S., Svitavská-Svobodová, H., Vannière, B., Tinner, W., 2018. The sedimentary and remote-sensing

reflection of biomass burning in Europe. Glob. Ecol. Biogeogr. 27, 199–212. https://doi.org/10.1111/geb.12682.
Aichner, B., Herzschuh, U., Wilkes, H., 2010. Influence of aquatic macrophytes on the stable carbon isotopic signatures of sedimentary organic matter in lakes on the Tibetan Plateau. Org. Geochem. 41, 706–718. https://doi.org/10.1016/j.orggeochem.2010.02.002.
Aichner, B., Ott, F., Słowiński, M., Noryśkiewicz, A.M., Brauer, A., Sachse, D., 2018. Leaf wax *n*-alkane distributions record ecological changes during the Younger Dryas at Trzechowskie paleolake (northern Poland) without temporal delay. Clim. Past 14, 1607–1624. https://doi.org/10.5194/cp-14-1607-2018.
Álvarez, M.C., Flores, J.A., Sierro, F.J., Diz, P., Francés, G., Pelejero, C., Grimalt, J., 2005. Millennial surface water dynamics in the Ría de Vigo during the last 3000 years as revealed by coccoliths and molecular biomarkers. Palaeogeogr. Palaeoclimatol. Palaeoecol. 218, 1–13. https://doi.org/10.1016/j.palaeo.2004.12.002.
Bartolomé, M., Moreno, A., Sancho, C., Cacho, I., Stoll, H., Haghipour, N., Belmonte, Á., Spötl, C., Hellstrom, J., Edwards, R.L., Cheng, H., 2024. Reconstructing hydroclimate changes over the past 2500 years using speleothems from Pyrenean caves (NE Spain). Clim. Past 20, 467–494. https://doi.org/10.5194/cp-20-467-2024.
Benali, A., Guiomar, N., Gonçalves, H., Mota, B., Silva, F., Fernandes, P.M., Mota, C., Penha, A., Santos, J., Pereira, J.M.C., Sá, A.C.L., 2023. The Portuguese large wildfire Spread database (PT-FireSprd). Earth Syst. Sci. Data 15, 3791–3818. https://doi.org/10.5194/essd-15-3791-2023.
Benito, G., Díez-Herrero, A., Fernández de Villalta, M., 2003. Magnitude and frequency of flooding in the Tagus basin (Central Spain) over the last millennium. Clim. Change 58, 171–192. https://doi.org/10.1023/A:1023417102053.
Bernárdez, P., González-Álvarez, R., Francés, G., Prego, R., Bárcena, M.A., Romero, O.E., 2008. Late Holocene history of the rainfall in the NW Iberian peninsula—evidence from a marine record. J. Mar. Syst., Oceanography of the Bay of Biscay 72, 366–382. https://doi.org/10.1016/j.jmarsys.2007.03.009.
Bindi, M., Olesen, J.E., 2011. The responses of agriculture in Europe to climate change. Reg. Environ. Change 11, 151–158. https://doi.org/10.1007/s10113-010-0173-x.
Blaauw, M., Christen, J.A., Bennett, K.D., Reimer, P.J., 2018. Double the dates and go for Bayes — impacts of model choice, dating density and quality on chronologies. Quat. Sci. Rev. 188, 58–66. https://doi.org/10.1016/j.quascirev.2018.03.032.
Boavida, M., Gliwicz, Z., 1996. Limnological and biological characteristics of the alpine lakes of Portugal. Limnética 12. https://doi.org/10.23818/limn.12.11.
Bowen, G.J., Cai, Z., Fiorella, R.P., Putman, A.L., 2019. Isotopes in the water cycle: regional- to global-scale patterns and Applications. Annu. Rev. Earth Planet Sci. 47, 453–479. https://doi.org/10.1146/annurev-earth-053018-060220.
Bray, E.E., Evans, E.D., 1961. Distribution of n-paraffins as a clue to recognition of source beds. Geochim. Cosmochim. Acta 22, 2–15. https://doi.org/10.1016/0016-7037(61)90069-2.
Brooks, S.J., Langdon, P.G., Heiri, O., 2007. The identification and use of Palaearctic Chironomidae larvae in palaeoecology. Quat. Res. Assoc. Tech. Guide i-vi 1.
Büntgen, U., Urban, O., Krusic, P.J., Rybníček, M., Kolář, T., Kyncl, T., Ač, A., Koňasová, E., Čáslavský, J., Esper, J., Wagner, S., Saurer, M., Tegel, W., Dobrovolný, P., Cherubini, P., Reinig, F., Trnka, M., 2021. Recent European drought extremes beyond Common Era background variability. Nat. Geosci. 14, 190–196. https://doi.org/10.1038/s41561-021-00698-0.
Campos, C., Couto, F.T., Filippi, J.-B., Baggio, R., Salgado, R., 2023. Modelling pyro-convection phenomenon during a mega-fire event in Portugal. Atmospheric Res 290, 106776. https://doi.org/10.1016/j.atmosres.2023.106776.
Carreira, P.M., Nunes, D., Valério, P., Araújo, M.F., 2009. A 15-year record of seasonal variation in the isotopic composition of precipitation water over continental Portugal. J. Radioanal. Nucl. Chem. 281, 153–156. https://doi.org/10.1007/s10967-009-0064-0.
Carrión, J.S., Fernández, S., González-Sampériz, P., Gil-Romera, G., Badal, E., Carrión-Marco, Y., López-Merino, L., López-Sáez, J.A., Fierro, E., Burjachs, F., 2010. Expected trends and surprises in the Lateglacial and holocene vegetation history of the iberian peninsula and Balearic Islands. Rev. Palaeobot. Palynol., Iberian Floras through Time: Land of Diversity and Survival 162, 458–475. https://doi.org/10.1016/j.revpalbo.2009.12.007.
Carrión, J.S., Munuera, M., Dupré, M., Andrade, A., 2001. Abrupt vegetation changes in the Segura mountains of southern Spain throughout the holocene. J. Ecol. 89, 783–797.
Chabaud, L., Sánchez Goñi, M.F., Desprat, S., Rossignol, L., 2014. Land–sea climatic variability in the eastern North Atlantic subtropical region over the last 14,200 years: atmospheric and oceanic processes at different timescales. Holocene 24, 787–797. https://doi.org/10.1177/0959683614530439.
Cheddadi, R., Carré, M., Nourelbait, M., François, L., Rhoujjati, A., Manay, R., Ochoa, D., Schefuß, E., 2021. Early Holocene greening of the Sahara requires Mediterranean winter rainfall. Proc. Natl. Acad. Sci. 118, e2024898118 https://doi.org/10.1073/pnas.2024898118.
Clark, J.S., Royall, P.D., 1996. Local and regional sediment charcoal evidence for fire regimes in Presettlement north-eastern north America. J. Ecol. 84, 365–382. https://doi.org/10.2307/2261199.
Comas-Bru, L., Hernández, A., 2018. Reconciling North Atlantic climate modes: revised monthly indices for the East Atlantic and the Scandinavian patterns beyond the 20th century. Earth Syst. Sci. Data 10, 2329–2344. https://doi.org/10.5194/essd-10-2329-2018.
Comas-Bru, L., McDermott, F., 2014. Impacts of the EA and SCA patterns on the European twentieth century NAO–winter climate relationship. Q. J. R. Meteorol. Soc. 140, 354–363. https://doi.org/10.1002/qj.2158.
Connor, S.E., Araújo, J., van der Knaap, W.O., van Leeuwen, J.F.N., 2012. A long-term perspective on biomass burning in the Serra da Estrela, Portugal. Quat. Sci. Rev. 55, 114–124. https://doi.org/10.1016/j.quascirev.2012.08.007.
Connor, S.E., van Leeuwen, J.F.N., van der Knaap, W.O. Pim, Akindola, R.B., Adeleye, M. A., Mariani, M., 2021. Pollen and plant diversity relationships in a Mediterranean montane area. Veg. Hist. Archaeobotany 30, 583–594. https://doi.org/10.1007/s00334-020-00811-0.
Corella, J.P., Stefanova, V., El Anjoumi, A., Rico, E., Giralt, S., Moreno, A., Plata-Montero, A., Valero-Garcés, B.L., 2013. A 2500-year multi-proxy reconstruction of climate change and human activities in northern Spain: the Lake Arreo record. Palaeogeogr. Palaeoclimatol. Palaeoecol. 386, 555–568. https://doi.org/10.1016/j.palaeo.2013.06.022.
Cortesi, N., Trigo, R.M., Gonzalez-Hidalgo, J.C., Ramos, A.M., 2013. Modelling monthly precipitation with circulation weather types for a dense network of stations over Iberia. Hydrol. Earth Syst. Sci. 17, 665–678. https://doi.org/10.5194/hess-17-665-2013.
Cresswell-Clay, N., Ummenhofer, C.C., Thatcher, D.L., Wanamaker, A.D., Denniston, R. F., Asmerom, Y., Polyak, V.J., 2022. Twentieth-century Azores High expansion unprecedented in the past 1,200 years. Nat. Geosci. 15, 548–553. https://doi.org/10.1038/s41561-022-00971-w.
Cui, D., Liang, S., Wang, D., Liu, Z., 2021. A 1 km global dataset of historical (1979–2013) and future (2020–2100) Köppen–Geiger climate classification and bioclimatic variables. Earth Syst. Sci. Data 13, 5087–5114. https://doi.org/10.5194/essd-13-5087-2021.
Curtis, C.J., Simpson, G.L., 2014. Trends in bulk deposition of acidity in the UK, 1988–2007, assessed using additive models. Ecol. Indic. 37, 274–286. https://doi.org/10.1016/j.ecolind.2012.10.023. Threats to upland waters.
Desprat, S., Sánchez Goñi, M.F., Loutre, M.-F., 2003. Revealing climatic variability of the last three millennia in northwestern Iberia using pollen influx data. Earth Planet Sci. Lett. 213, 63–78. https://doi.org/10.1016/S0012-821X(03)00292-9.
Espinha Marques, J., Samper, J., Pisani, B., Alvares, D., Carvalho, J.M., Chaminé, H.I., Marques, J.M., Vieira, G.T., Mora, C., Sodré Borges, F., 2011. Evaluation of water resources in a high-mountain basin in Serra da Estrela, Central Portugal, using a semi-distributed hydrological model. Environ. Earth Sci. 62, 1219–1234. https://doi.org/10.1007/s12665-010-0610-7.
Fagúndez, J., Pontevedra-Pombal, X., 2022. Soil properties of North Iberian wet heathlands in relation to climate, management and plant community. Plant Soil 475, 565–580. https://doi.org/10.1007/s11104-022-05393-6.
Farquhar, G.D., Hubick, K.T., Condon, A.G., Richards, R.A., 1989. Carbon isotope fractionation and plant water-use efficiency. In: Rundel, P.W., Ehleringer, J.R., Nagy, K.A. (Eds.), Stable Isotopes in Ecological Research. Springer, New York, NY, pp. 21–40. https://doi.org/10.1007/978-1-4612-3498-2_2.
Ficken, K.J., Li, B., Swain, D.L., Eglinton, G., 2000. An n-alkane proxy for the sedimentary input of submerged/floating freshwater aquatic macrophytes. Org. Geochem. 31, 745–749. https://doi.org/10.1016/S0146-6380(00)00081-4.
Finsinger, W., Tinner, W., 2005. Minimum count sums for charcoal concentration estimates in pollen slides: accuracy and potential errors. Holocene 15, 293–297. https://doi.org/10.1191/0959683605hl808rr.
Fletcher, W., Carrión, J.S., Fernández, S., González-Sampériz, P., López-Merino, L., Peña, L., Burjachs, F., López-Sáez, J.A., García-Antón, M., Marco, Y.C., Uzquiano, P., Postigo, J.M., Barrón, E., Allué, E., Badal, E., Dupré, M., Fierro, E., Munuera, M., Rubiales, J.M., Amorena, I.G., Moreno, G.J., Romera, G.G., Leroy, S., García-Martínez, M.S., Montoya, E., Yll, E., Vieira, M., Rodríguez-Ariza, M.O., Anderson, S., Peñalba, C., García, M.J.G., Sanz, A.P., Albert, R.M., Díez, M.J., Morales, C., Manzaneque, F.G., Parra, I., Zapata, B.R., Riera, S., Zapata, L., Ejarque, A., Vegas, T., Rull, V., Scott, L., Andrade, A., Díaz, S.P., Schaad, D.A., Moreno, E., Hernández-Mateo, L., Baena, J.J.S., Riquelme, J.A., Iglesias, R., Franco, F., Chaín, C., Figueiral, I., Grau, E., Matos, M., Espejo, F.J., Arribas, A., Garrido, G., Finlayson, G., Finlayson, C., Ruiz, M., Jordá, G.P., Miras, Y., 2012. Paleoflora y Paleovegetación de la Península Ibérica e Islas Baleares: Plioceno-Cuaternario.
García-Alix, A., Camuera, J., Ramos-Román, M.J., Toney, J.L., Sachse, D., Schefuß, E., Jiménez-Moreno, G., Jiménez-Espejo, F.J., López-Avilés, A., Anderson, R.S., Yanes, Y., 2021. Paleohydrological dynamics in the Western Mediterranean during the last glacial cycle. Glob. Planet. Change 202, 103527. https://doi.org/10.1016/j.gloplacha.2021.103527.
García-Alix, A., Jiménez-Espejo, F.J., Toney, J.L., Jiménez-Moreno, G., Ramos-Román, M.J., Anderson, R.S., Ruano, P., Queralt, I., Delgado Huertas, A., Kuroda, J., 2017. Alpine bogs of southern Spain show human-induced environmental change superimposed on long-term natural variations. Sci. Rep. 7, 7439. https://doi.org/10.1038/s41598-017-07854-w.
García-Alix, A., Toney, J.L., Jiménez-Moreno, G., Pérez-Martínez, C., Jiménez, L., Rodrigo-Gámiz, M., Anderson, R.S., Camuera, J., Jiménez-Espejo, F.J., Peña-Angulo, D., Ramos-Román, M.J., 2020. Algal lipids reveal unprecedented warming rates in alpine areas of SW Europe during the industrial period. Clim. Past 16, 245–263. https://doi.org/10.5194/cp-16-245-2020.
Gázquez, F., Bauska, T.K., Comas-Bru, L., Ghaleb, B., Calaforra, J.-M., Hodell, D.A., 2020. The potential of gypsum speleothems for paleoclimatology: application to the Iberian Roman Humid Period. Sci. Rep. 10, 14705 https://doi.org/10.1038/s41598-020-71679-3.
Gerten, D., Adrian, R., 2001. Differences in the persistency of the North Atlantic Oscillation signal among lakes. Limnol. Oceanogr. 46, 448–455. https://doi.org/10.4319/lo.2001.46.2.0448.
Gil García, M.J., Ruiz Zapata, M.B., Santisteban, J.I., Mediavilla, R., López-Pamo, E., Dabrio, C.J., 2007. Late holocene environments in Las Tablas de Daimiel (south central Iberian peninsula, Spain). Veg. Hist. Archaeobotany 16, 241–250. https://doi.org/10.1007/s00334-006-0047-9.
Gil-Romera, G., Adolf, C., Benito, B.M., Bittner, L., Johansson, M.U., Grady, D.A., Lamb, H.F., Lemma, B., Fekadu, M., Glaser, B., Mekonnen, B., Sevilla-Callejo, M., Zech, M., Zech, W., Miehe, G., 2019. Long-term fire resilience of the Ericaceous Belt,

Bale mountains, Ethiopia. Biol. Lett. 15, 20190357 https://doi.org/10.1098/rsbl.2019.0357.
Hernández, A., Parnell, A., Cahill, N., Geyer, A., Trigo, R.M., Giralt, S., 2020. A 2,000-year Bayesian NAO reconstruction from the Iberian Peninsula. Sci. Rep. 10 (1), 1–15. https://doi.org/10.1038/s41598-020-71372-5.
Hernández, A., Sáez, A., Santos, R.N., Rodrigues, T., Martin-Puertas, C., Gil-Romera, G., Abbott, M., Carballeira, R., Costa, P., Giralt, S., Gomes, S.D., Griffore, M., Ibañez-Insa, J., Leira, M., Moreno, J., Naughton, F., Oliveira, D., Raposeiro, P.M., Trigo, R. M., Vieira, G., Ramos, A.M., 2023. The timing of the deglaciation in the Atlantic Iberian mountains: Insights from the stratigraphic analysis of a lake sequence in Serra da Estrela (Portugal). Earth Surf. Process. Landf. 48, 233–242. https://doi.org/10.1002/esp.5536.
Hernández, A., Trigo, R.M., Pla-Rabes, S., Valero-Garcés, B.L., Jerez, S., Rico-Herrero, M., Vega, J.C., Jambrina-Enríquez, M., Giralt, S., 2015. Sensitivity of two Iberian lakes to North Atlantic atmospheric circulation modes. Clim. Dyn. 45, 3403–3417. https://doi.org/10.1007/s00382-015-2547-8.
Higuera, P.E., Gavin, D.G., Bartlein, P.J., Hallett, D.J., 2010. Peak detection in sediment–charcoal records: impacts of alternative data analysis methods on fire-history interpretations. Int. J. Wildland Fire 19, 996–1014. https://doi.org/10.1071/WF09134.
Hou, J., D'Andrea, W.J., MacDonald, D., Huang, Y., 2007. Evidence for water use efficiency as an important factor in determining the δD values of tree leaf waxes. Org. Geochem. 38, 1251–1255. https://doi.org/10.1016/j.orggeochem.2007.03.011.
Hurrell, J.W., 1995. Decadal trends in the North Atlantic oscillation: regional temperatures and precipitation. Science 269, 676–679. https://doi.org/10.1126/science.269.5224.676.
Jalut, G., Esteban Amat, A., Bonnet, L., Gauquelin, T., Fontugne, M., 2000. Holocene climatic changes in the Western Mediterranean, from south-east France to south-east Spain. Palaeogeogr. Palaeoclimatol. Palaeoecol. 160, 255–290. https://doi.org/10.1016/S0031-0182(00)00075-4.
Jambrina-Enríquez, M., Rico, M., Moreno, A., Leira, M., Bernárdez, P., Prego, R., Recio, C., Valero-Garcés, B.L., 2014. Timing of deglaciation and postglacial environmental dynamics in NW Iberia: the Sanabria Lake record. Quat. Sci. Rev. 94, 136–158. https://doi.org/10.1016/j.quascirev.2014.04.018.
Jansen, J., 2011. Managing Natura 2000 in a changing world : the case of the Serra da Estrela (Portugal). S.l : s.n.
Jiménez-Moreno, G., García-Alix, A., Hernández-Corbalán, M.D., Anderson, R.S., Delgado-Huertas, A., 2013. Vegetation, fire, climate and human disturbance history in the southwestern Mediterranean area during the late Holocene. Quat. Res. 79, 110–122. https://doi.org/10.1016/j.yqres.2012.11.008.
Kahmen, A., Schefuß, E., Sachse, D., 2013. Leaf water deuterium enrichment shapes leaf wax n-alkane δD values of angiosperm plants I: Experimental evidence and mechanistic insights. Geochimica et Cosmochimica Acta 111, 39–49. https://doi.org/10.1016/j.gca.2012.09.003.
Lei, Y., Wang, Y., Qin, F., Liu, J., Feng, P., Luo, L., Jordan, R.W., Jiang, S., 2021. Diatom assemblage shift driven by nutrient dynamics in a large, subtropical reservoir in southern China. J. Clean. Prod. 317, 128435 https://doi.org/10.1016/j.jclepro.2021.128435.
Leira, M., Chen, G., Dalton, C., Irvine, K., Taylor, D., 2009. Patterns in freshwater diatom taxonomic distinctness along an eutrophication gradient. Freshw. Biol. 54, 1–14. https://doi.org/10.1111/j.1365-2427.2008.02086.x.
Leira, M., Sabater, S., 2005. Diatom assemblages distribution in Catalan rivers, NE Spain, in relation to chemical and physiographical factors. Water Res. 39, 73–82. https://doi.org/10.1016/j.watres.2004.08.034.
Lionello, P., 2012. The Climate of the Mediterranean Region: from the Past to the Future. Elsevier insights. Elsevier Science.
Liu, J., An, Z., 2019. Variations in hydrogen isotopic fractionation in higher plants and sediments across different latitudes: implications for paleohydrological reconstruction. Sci. Total Environ. 650, 470–478. https://doi.org/10.1016/j.scitotenv.2018.09.047.
López-Avilés, A., García-Alix, A., Jiménez-Moreno, G., Anderson, R.S., Toney, J.L., Mesa-Fernández, J.M., Jiménez-Espejo, F.J., 2021. Latest Holocene paleoenvironmental and paleoclimate reconstruction from an alpine bog in the Western Mediterranean region: The Borreguil de los Lavaderos de la Reina record (Sierra Nevada). Palaeogeogr. Palaeoclimatol. Palaeoecol. 573, 110434 https://doi.org/10.1016/j.palaeo.2021.110434.
López-Avilés, A., Jiménez-Moreno, G., García-Alix, A., García-García, F., Camuera, J., Scott Anderson, R., Sanjurjo-Sánchez, J., Arce Chamorro, C., Carrión, J.S., 2022. Post-glacial evolution of alpine environments in the western Mediterranean region: the Laguna Seca record. Catena 211, 106033. https://doi.org/10.1016/j.catena.2022.106033.
López-Merino, L., López-Sáez, J.A., Alba-Sánchez, F., Pérez-Díaz, S., Carrión, J.S., 2009. 2000 years of pastoralism and fire shaping high-altitude vegetation of Sierra de Gredos in central Spain. Rev. Palaeobot. Palynol. 158, 42–51. https://doi.org/10.1016/j.revpalbo.2009.07.003.
Lunn, D., Jackson, C., Best, N., Thomas, A., Spiegelhalter, D., 2012. The BUGS Book: A Practical Introduction to Bayesian Analysis. CRC Press.
Marlon, J.R., Bartlein, P.J., Gavin, D.G., Long, C.J., Anderson, R.S., Briles, C.E., Brown, K. J., Colombaroli, D., Hallett, D.J., Power, M.J., Scharf, E.A., Walsh, M.K., 2012. Long-term perspective on wildfires in the western USA. Proc. Natl. Acad. Sci. 109, E535–E543. https://doi.org/10.1073/pnas.1112839109.
Marques, J.E., Marques, J.M., Chaminé, H.I., Carreira, P.M., Fonseca, P.E., Monteiro Santos, F.A., Moura, R., Samper, J., Pisani, B., Teixeira, J., Carvalho, J.M., Rocha, F., Borges, F.S., 2013. Conceptualizing a mountain hydrogeologic system by using an integrated groundwater assessment (Serra da Estrela, Central Portugal): a review. Geosci. J. 17, 371–386. https://doi.org/10.1007/s12303-013-0019-x.
Martín-Chivelet, J., Muñoz-García, M.B., Edwards, R.L., Turrero, M.J., Ortega, A.I., 2011. Land surface temperature changes in Northern Iberia since 4000yrBP, based on δ13C of speleothems. Glob. Planet. Change 77, 1–12. https://doi.org/10.1016/j.gloplacha.2011.02.002.
Martín-Puertas, C., Valero-Garcés, B.L., Pilar Mata, M., González-Sampériz, P., Bao, R., Moreno, A., Stefanova, V., 2008. Arid and humid phases in southern Spain during the last 4000 years: the Zoñar Lake record, Córdoba. Holocene 18, 907–921. https://doi.org/10.1177/0959683608093533.
Marzi, R., Torkelson, B.E., Olson, R.K., 1993. A revised carbon preference index. Org. Geochem. 20, 1303–1306. https://doi.org/10.1016/0146-6380(93)90016-5.
McVicar, T.R., Roderick, M.L., Donohue, R.J., Van Niel, T.G., 2012. Less bluster ahead? Ecohydrological implications of global trends of terrestrial near-surface wind speeds. Ecohydrology 5, 381–388. https://doi.org/10.1002/eco.1298.
Mellado-Cano, J., Barriopedro, D., García-Herrera, R., Trigo, R.M., Hernández, A., 2019. Examining the North Atlantic oscillation, East Atlantic pattern, and jet variability since 1685. J. Clim. 32, 6285–6298. https://doi.org/10.1175/JCLI-D-19-0135.1.
Molina, J.A., 2017. Aquatic and Wetland vegetation of the iberian peninsula. In: Loidi, J. (Ed.), The Vegetation of the Iberian Peninsula: Volume 2, Plant and Vegetation. Springer International Publishing, Cham, pp. 355–396. https://doi.org/10.1007/978-3-319-54867-8_7.
Moore, P.D., Webb, J.A., Collison, M.E., 1991. Pollen Analysis. Pollen Anal.
Mora, C., 2010. A synthetic map of the climatopes of the Serra da Estrela (Portugal). J. Maps 6, 591–608. https://doi.org/10.4113/jom.2010.1112.
Morellón, M., Valero-Garcés, B., González-Sampériz, P., Vegas-Vilarrúbia, T., Rubio, E., Rieradevall, M., Delgado-Huertas, A., Mata, P., Romero, Ó., Engstrom, D.R., López-Vicente, M., Navas, A., Soto, J., 2011. Climate changes and human activities recorded in the sediments of Lake Estanya (NE Spain) during the Medieval warm period and Little Ice age. J. Paleolimnol. 46, 423–452. https://doi.org/10.1007/s10933-009-9346-3.
Moreno, A., Pérez, A., Frigola, J., Nieto-Moreno, V., Rodrigo-Gámiz, M., Martrat, B., González-Sampériz, P., Morellón, M., Martín-Puertas, C., Corella, J.P., Belmonte, Á., Sancho, C., Cacho, I., Herrera, G., Canals, M., Grimalt, J.O., Jiménez-Espejo, F., Martínez-Ruiz, F., Vegas-Vilarrúbia, T., Valero-Garcés, B.L., 2012. The Medieval climate anomaly in the iberian peninsula reconstructed from marine and lake records. Quat. Sci. Rev. 43, 16–32. https://doi.org/10.1016/j.quascirev.2012.04.007.
Moreno, J., Ramos, A.M., Raposeiro, P.M., Santos, R.N., Rodrigues, T., Naughton, F., Moreno, F., Trigo, R.M., Ibañez-Insa, J., Ludwig, P., Shi, X., Hernández, A., 2023. Identifying imprints of externally derived dust and halogens in the sedimentary record of an Iberian alpine lake for the past ~13,500 years – Lake Peixão, Serra da Estrela (Central Portugal). Sci. Total Environ. 903, 166179 https://doi.org/10.1016/j.scitotenv.2023.166179.
Naughton, F., Costas, S., Gomes, S.D., Desprat, S., Rodrigues, T., Sanchez Goñi, M.F., Renssen, H., Trigo, R., Bronk-Ramsey, C., Oliveira, D., Salgueiro, E., Voelker, A.H.L., Abrantes, F., 2019. Coupled ocean and atmospheric changes during Greenland stadial 1 in southwestern Europe. Quat. Sci. Rev. 212, 108–120. https://doi.org/10.1016/j.quascirev.2019.03.033.
Naughton, F., Sanchez Goñi, M.F., Desprat, S., Turon, J.-L., Duprat, J., Malaizé, B., Joli, C., Cortijo, E., Drago, T., Freitas, M.C., 2007. Present-day and past (last 25000 years) marine pollen signal off western Iberia. Mar. Micropaleontol. 62, 91–114. https://doi.org/10.1016/j.marmicro.2006.07.006.
Naughton, F., Sanchez Goñi, M.F., Rodrigues, T., Salgueiro, E., Costas, S., Desprat, S., Duprat, J., Michel, E., Rossignol, L., Zaragosi, S., Voelker, A.H.L., Abrantes, F., 2016. Climate variability across the last deglaciation in NW Iberia and its margin. Quat. Int. 414, 9–22. https://doi.org/10.1016/j.quaint.2015.08.073.
Oliva, M., Ruiz-Fernández, J., Barriendos, M., Benito, G., Cuadrat, J.M., Domínguez-Castro, F., García-Ruiz, J.M., Giralt, S., Gómez-Ortiz, A., Hernández, A., López-Costas, O., López-Moreno, J.I., López-Sáez, J.A., Martínez-Cortizas, A., Moreno, A., Prohom, M., Saz, M.A., Serrano, E., Tejedor, E., Trigo, R., Valero-Garcés, B., Vicente-Serrano, S.M., 2018. The Little Ice age in iberian mountains. Earth Sci. Rev. 177, 175–208. https://doi.org/10.1016/j.earscirev.2017.11.010.
Oliveira, D., Sánchez Goñi, M.F., Naughton, F., Polanco-Martínez, J.M., Jimenez-Espejo, F.J., Grimalt, J.O., Martrat, B., Voelker, A.H.L., Trigo, R., Hodell, D., Abrantes, F., Desprat, S., 2017. Unexpected weak seasonal climate in the western Mediterranean region during MIS 31, a high-insolation forced interglacial. Quat. Sci. Rev. 161, 1–17. https://doi.org/10.1016/j.quascirev.2017.02.013.
Ortiz, J.E., Moreno, L., Torres, T., Vegas, J., Ruiz-Zapata, B., García-Cortés, Á., Galán, L., Pérez-González, A., 2013. A 220 ka palaeoenvironmental reconstruction of the Fuentillejo maar lake record (Central Spain) using biomarker analysis. Organic Geochemistry 55, 85–97. https://doi.org/10.1016/j.orggeochem.2012.11.012.
Pancost, R.D., Boot, C.S., 2004. The Palaeoclimatic Utility of Terrestrial Biomarkers in Marine Sediments. Mar. Chem., New Approaches in Marine Organic Biogeochemistry: A Tribute to the Life and Science of John I, vol. 92. Hedges, pp. 239–261. https://doi.org/10.1016/j.marchem.2004.06.029.
Pienitz, R., Smol, J.P., Birks, H.J.B., 1995. Assessment of freshwater diatoms as quantitative indicators of past climatic change in the Yukon and Northwest Territories, Canada. J. Paleolimnol. 13, 21–49. https://doi.org/10.1007/BF00678109.
Plummer, M., 2012. JAGS: just another Gibbs sampler. Astrophys. Source Code Libr. ascl: 1209.002.
Poynter, J.G., Farrimond, P., Robinson, N., Eglinton, G., 1989. Aeolian-derived higher plant lipids in the marine sedimentary record: Links with Palaeoclimate. In: Leinen, M., Sarnthein, M. (Eds.), Paleoclimatology and Paleometeorology: Modern and Past Patterns of Global Atmospheric Transport, NATO ASI Series. Springer,

Netherlands, Dordrecht, pp. 435–462. https://doi.org/10.1007/978-94-009-0995-3_18.
Råman Vinnå, L., Medhaug, I., Schmid, M., Bouffard, D., 2021. The vulnerability of lakes to climate change along an altitudinal gradient. Commun. Earth Environ. 2, 1–10. https://doi.org/10.1038/s43247-021-00106-w.
Reille, M., 1992. Pollen et spores d'Europe et d'Afrique du Nord. Laboratoire de Botanique Historique et Palynologie.
Rühland, K., Paterson, A.M., Smol, J.P., 2008. Hemispheric-scale patterns of climate-related shifts in planktonic diatoms from North American and European lakes. Glob. Change Biol. 14, 2740–2754. https://doi.org/10.1111/j.1365-2486.2008.01670.x.
Rühland, K., Priesnitz, A., Smol, J.P., 2003. Paleolimnological evidence from diatoms for recent environmental changes in 50 lakes across Canadian Arctic Treeline. Arct. Antarct. Alp. Res. 35, 110–123. https://doi.org/10.1657/1523-0430(2003)035[0110:PEFDFR]2.0.CO;2.
Sachse, D., Billault, I., Bowen, G.J., Chikaraishi, Y., Dawson, T.E., Feakins, S.J., Freeman, K.H., Magill, C.R., McInerney, F.A., van der Meer, M.T.J., Polissar, P., Robins, R.J., Sachs, J.P., Schmidt, H.-L., Sessions, A.L., White, J.W.C., West, J.B., Kahmen, A., 2012. Molecular Paleohydrology: interpreting the hydrogen-isotopic composition of lipid biomarkers from Photosynthesizing Organisms. Annu. Rev. Earth Planet Sci. 40, 221–249. https://doi.org/10.1146/annurev-earth-042711-105535.
Sánchez-López, G., Hernández, A., Pla-Rabes, S., Trigo, R.M., Toro, M., Granados, I., Sáez, A., Masqué, P., Pueyo, J.J., Rubio-Inglés, M.J., Giralt, S., 2016. Climate reconstruction for the last two millennia in central iberia: the role of East Atlantic (EA), North Atlantic oscillation (NAO) and their interplay over the iberian peninsula. Quat. Sci. Rev. 149, 135–150. https://doi.org/10.1016/j.quascirev.2016.07.021.
Sánchez-Mata, D., Gavilán, R.G., de la Fuente, V., 2017. The Sistema central (central range). In: Loidi, J. (Ed.), The Vegetation of the Iberian Peninsula: Volume 1, Plant and Vegetation. Springer International Publishing, Cham, pp. 549–588. https://doi.org/10.1007/978-3-319-54784-8_13.
Santos, R.N., 2021. Hydroclimate of Western Iberia over the last 2000 years: Insights from leaf wax n-alkanes of Lake Peixão sediments (Serra da Estrela, Portugal) (masterThesis).
Santos, R.N., Schefuß, E., Cordeiro, L.G.M.S., Oliveira, D., Hernández, A., Ramos, A.M., Rodrigues, T., 2022. Leaf wax biomarkers of a high-mountain lake area in western iberia—implications for environmental reconstructions. Front. Environ. Sci. 10.
Schwörer, C., Morales-Molino, C., Gobet, E., Henne, P.D., Pasta, S., Pedrotta, T., van Leeuwen, J.F.N., Vannière, B., Tinner, W., n.d. Simulating past and future fire impacts on Mediterranean ecosystems. J. Ecol. n/a. https://doi.org/10.1111/1365-2745.14293.
Scussolini, P., Vegas-Vilarrúbia, T., Rull, V., Corella, J.P., Valero-Garcés, B., Gomà, J., 2011. Middle and late Holocene climate change and human impact inferred from diatoms, algae and aquatic macrophyte pollen in sediments from Lake Montcortès (NE Iberian Peninsula). J. Paleolimnol. 46, 369–385. https://doi.org/10.1007/s10933-011-9524-y.
Serrano, A., Mateos, V.L., Garcia, J.A., 1999. Trend analysis of monthly precipitation over the iberian peninsula for the period 1921–1995. Phys. Chem. Earth Part B Hydrol. Oceans Atmosphere, European Water Resources and Climate Changes Processes 24, 85–90. https://doi.org/10.1016/S1464-1909(98)00016-1.
Simpson, G.L., 2018. Modelling Palaeoecological time series using Generalised additive models. Front. Ecol. Evol. 6.
Simpson, G., 2024. gratia: Graceful ggplot-Based Graphics and Other Functions for GAMs Fitted using mgcv. R package version 0.9.2.9002. https://gavinsimpson.github.io/gratia/.
Sousa, P.M., Ramos, A.M., Raible, C.C., Messmer, M., Tomé, R., Pinto, J.G., Trigo, R.M., 2020. North Atlantic integrated water Vapor Transport—from 850 to 2100 CE: impacts on western European rainfall. J. Clim. 33, 263–279. https://doi.org/10.1175/JCLI-D-19-0348.1.
Taylor, A.K., Benedetti, M.M., Haws, J.A., Lane, C.S., 2018. Mid-Holocene Iberian hydroclimate variability and paleoenvironmental change: molecular and isotopic insights from Praia Rei Cortiço, Portugal. J. Quat. Sci. 33, 79–92. https://doi.org/10.1002/jqs.3000.
Tedim, F., Remelgado, R., Borges, C., Carvalho, S., Martins, J., 2013. Exploring the occurrence of mega-fires in Portugal. For. Ecol. Manag. Mega-fire Reality 294, 86–96. https://doi.org/10.1016/j.foreco.2012.07.031.
Thatcher, D.L., Wanamaker, A.D., Denniston, R.F., Asmerom, Y., Polyak, V.J., Fullick, D., Ummenhofer, C.C., Gillikin, D.P., Haws, J.A., 2020. Hydroclimate variability from western Iberia (Portugal) during the Holocene: insights from a composite stalagmite isotope record. Holocene 30, 966–981. https://doi.org/10.1177/0959683620908648.
Thatcher, D.L., Wanamaker, A.D., Denniston, R.F., Ummenhofer, C.C., Asmerom, Y., Polyak, V.J., Cresswell-Clay, N., Hasiuk, F., Haws, J., Gillikin, D.P., 2023. Iberian hydroclimate variability and the Azores High during the last 1200 years: evidence from proxy records and climate model simulations. Clim. Dyn. 60, 2365–2387. https://doi.org/10.1007/s00382-022-06427-6.
Tian, Q., Huang, G., Hu, K., Niyogi, D., 2019. Observed and global climate model based changes in wind power potential over the Northern Hemisphere during 1979–2016. Energy 167, 1224–1235. https://doi.org/10.1016/j.energy.2018.11.027.
Tinner, W., Hu, F.S., 2003. Size parameters, size-class distribution and area-number relationship of microscopic charcoal: relevance for fire reconstruction. Holocene 13, 499–505. https://doi.org/10.1191/0959683603hl615rp.
Toney, J.L., García-Alix, A., Jiménez-Moreno, G., Anderson, R.S., Moossen, H., Seki, O., 2020. New insights into Holocene hydrology and temperature from lipid biomarkers in western Mediterranean alpine wetlands. Quat. Sci. Rev. 240, 106395 https://doi.org/10.1016/j.quascirev.2020.106395.
Trigo, R.M., Osborn, T.J., Corte-Real, J.M., 2002. The North Atlantic Oscillation influence on Europe: climate impacts and associated physical mechanisms. Clim. Res. 20, 9–17. https://doi.org/10.3354/cr020009.
Trigo, R.M., Pozo-Vázquez, D., Osborn, T.J., Castro-Díez, Y., Gámiz-Fortis, S., Esteban-Parra, M.J., 2004. North Atlantic oscillation influence on precipitation, river flow and water resources in the Iberian Peninsula. Int. J. Climatol. 24, 925–944. https://doi.org/10.1002/joc.1048.
Trigo, R.M., Valente, M.A., Trigo, I.F., Miranda, P.M.A., Ramos, A.M., Paredes, D., García-Herrera, R., 2008. The impact of North Atlantic wind and Cyclone trends on European precipitation and significant wave Height in the Atlantic. Ann. N. Y. Acad. Sci. 1146, 212–234. https://doi.org/10.1196/annals.1446.014.
Turner, R., Kelly, A., Roberts, N., 2004. A critical assessment and experimental comparison of microscopic charcoal extraction methods. Charcoals Past Cult. Palaeoenvironmental Implic. Proc. Third Int. Meet. Anthracology 265–272.
Ulbrich, U., Christoph, M., Pinto, J.g., Corte-Real, J., 1999. Dependence of winter precipitation over Portugal on NAO and baroclinic wave activity. Int. J. Climatol. 19, 379–390. https://doi.org/10.1002/(SICI)1097-0088(19990330)19:4<379::AID-JOC357>3.0.CO;2-8.
van der Knaap, W.O., van Leeuwen, J.F.N., 1997. Late Glacial and early Holocene vegetation succession, altitudinal vegetation zonation, and climatic change in the Serra da Estrela. Portugal. Rev. Palaeobot. Palynol. 97, 239–285. https://doi.org/10.1016/S0034-6667(97)00008-0.
van der Knaap, W., Van Leeuwen, J., 1995. Holocene vegetation succession and degradation as responses to climatic change and human activity in the Serra de Estrela, Portugal. Rev. Palaeobot. Palynol. 89 (3–4), 153–211. https://doi.org/10.1016/0034-6667(95)00048-0.
van der Knaap, W.O., van Leeuwen, J.F.N., 1995. Holocene vegetation succession and degradation as responses to climatic change and human activity in the Serra de Estrela. Portugal. Rev. Palaeobot. Palynol. 89, 153–211. https://doi.org/10.1016/0034-6667(95)00048-0.
Vázquez-Loureiro, D., Sáez, A., Gonçalves, V., Buchaca, T., Hernández, A., Raposeiro, P. M., de Boer, E.J., Masqué, P., Giralt, S., Bao, R., 2023. Recent global warming induces the coupling of dissimilar long-term sedimentary signatures in two adjacent volcanic lakes (Azores Archipelago, Portugal). Quat. Sci. Rev. 303, 107968 https://doi.org/10.1016/j.quascirev.2023.107968.
Vieira, G., 2008. Combined numerical and geomorphological reconstruction of the Serra da Estrela plateau icefield, Portugal. Geomorphology, Glacial Landscape Evolution - Implications for Glacial Processes. Patterns and Reconstructions 97, 190–207. https://doi.org/10.1016/j.geomorph.2007.02.042.
Vieira, G., Nieuwendam, A., 2020. Glacial and Periglacial Landscapes of the Serra da Estrela. In: Vieira, G., Zêzere, J.L., Mora, C. (Eds.), Landscapes and Landforms of Portugal, World Geomorphological Landscapes. Springer International Publishing, Cham, pp. 185–198. https://doi.org/10.1007/978-3-319-03641-0_15.
Villanueva, J., Grimalt, J.O., Cortijo, E., Vidal, L., Labeyriez, L., 1997. A biomarker approach to the organic matter deposited in the North Atlantic during the last climatic cycle. Geochim. Cosmochim. Acta 61, 4633–4646. https://doi.org/10.1016/S0016-7037(97)83123-7.
Wanner, H., Brönnimann, S., Casty, C., Gyalistras, D., Luterbacher, J., Schmutz, C., Stephenson, D.B., Xoplaki, E., 2001. North Atlantic oscillation – Concepts and studies. Surv. Geophys. 22, 321–381. https://doi.org/10.1023/A:1014217317898.
Wiesenberg, G.L.B., Schwarzbauer, J., Schmidt, M.W.I., Schwark, L., 2004. Source and turnover of organic matter in agricultural soils derived from *n*-alkane/*n*-carboxylic acid compositions and C-isotope signatures, 35. In: Org. Geochem., Advances in Organic Geochemistry 2003. Proceedings of the 21st International Meeting on Organic Geochemistry, pp. 1371–1393. https://doi.org/10.1016/j.orggeochem.2004.03.009.
Wood, S.N., 2017. Generalized Additive Models: an Introduction with R, second ed. CRC Press.
Xie, S., Guo, J., Huang, J., Chen, F., Wang, H., Farrimond, P., 2004. Restricted utility of δ13C of bulk organic matter as a record of paleovegetation in some loess–paleosol sequences in the Chinese Loess Plateau. Quat. Res. 62 (1), 86–93. https://doi.org/10.1016/j.yqres.2004.03.004.
Yang, D., Bowen, G.J., 2022. Integrating plant wax abundance and isotopes for paleo-vegetation and paleoclimate reconstructions: a multi-source mixing model using a Bayesian framework. Clim. Past 18, 2181–2210. https://doi.org/10.5194/cp-18-2181-2022.
Zubiate, L., McDermott, F., Sweeney, C., O'Malley, M., 2017. Spatial variability in winter NAO–wind speed relationships in western Europe linked to concomitant states of the East Atlantic and Scandinavian patterns. Q. J. R. Meteorol. Soc. 143, 552–562. https://doi.org/10.1002/qj.2943.